

LOW AND HIGH IONIZATION ABSORPTION PROPERTIES OF Mg II ABSORPTION-SELECTED
GALAXIES AT INTERMEDIATE REDSHIFTS. I. GENERAL PROPERTIES^{1,2}CHRISTOPHER W. CHURCHILL³, RICHARD R. MELLON, JANE C. CHARLTON⁴

The Pennsylvania State University, University Park, PA 16802

BUELL T. JANNUZI

National Optical Astronomy Observatories, Tucson, AZ 85719

SOFIA KIRHAKOS

Institute for Advanced Study, Princeton, NJ 08544

CHARLES C. STEIDEL⁵

California Institute of Technology, Palomar Observatories, Pasadena, CA 91125

AND

DONALD P. SCHNEIDER

The Pennsylvania State University, University Park, PA 16802

The Astrophysical Journal, in press

ABSTRACT

We present extensive metal-line absorption properties for 45 absorption systems that were selected by their Mg II absorption at redshifts between 0.4 and 1.4. For each system the properties of several chemical species are determined, including a wide range of ionization conditions. In the optical, the absorption systems have been observed at $\sim 6 \text{ km s}^{-1}$ resolution with HIRES/Keck, which covered Mg II, several Fe II transitions, Mg I, and in some cases (depending upon redshift), Ca II, Ti II, Mn II, and Al III. Ultraviolet, lower resolution ($\sim 230 \text{ km s}^{-1}$) Faint Object Spectrograph data (1600 Å–3275 Å) were obtained from the *Hubble Space Telescope* archive. These spectra covered Al II, Al III, Si II, Si III, Si IV, C II, C III, C IV, N V, O VI, and several Lyman series transitions, with coverage dependent upon the absorption system redshift. From these data, we infer that Mg II absorbing galaxies at intermediate redshifts have multiphase gaseous structures.

Subject headings: quasars—absorption lines; galaxies—evolution; galaxies—halos

1. INTRODUCTION

During the last decade a great deal of progress has been made toward understanding the physical properties of intervening metal-line absorption systems measured in the spectra of high redshift quasars. This is particularly true at intermediate redshifts, $0.5 \leq z \leq 1.5$, for absorbers selected by the presence of the resonant Mg II $\lambda\lambda 2796, 2803$ doublet (e.g. Lanzetta, Turnshek, & Wolfe 1987; Tytler et al. 1987; Sargent, Boksenberg, & Steidel 1988; Petitjean & Bergeron 1990, Steidel & Sargent 1992). One of the most notable achievements was the demonstration that Mg II absorbers with $W_r(2796) \geq 0.3 \text{ \AA}$ are almost always associated with galaxies (Bergeron & Boissé 1991; Steidel 1995). Those works substantiated the ~ 30 -year standing hypothesis by Bahcall & Spitzer (1969) that metal-line absorption in quasar spectra arises in extended gaseous envelopes surrounding intervening galaxies.

The general picture today is that a wide variety of morphological types (from ellipticals to irregulars) have gaseous “halos” that extend to roughly 40 kpc, with the most common being Sbc–Scd types (Steidel, Dickinson, & Persson 1994; Guillemin & Bergeron 1997). The line-of-sight gas kinematics of the absorbers is consistent with that expected for material bound in

galactic potential wells (Petitjean & Bergeron 1990; Churchill, Steidel, & Vogt 1996; Charlton & Churchill 1998). This picture, however, is not without its counter examples or ambiguities. In some cases there is evidence that compact star forming objects spread out over ~ 200 kpc are seen at the Mg II absorption redshift and there is no directly associable bright galaxy (Yanny 1992; Yanny & York 1992). It is also not yet established whether the more numerous “weak” Mg II absorbers, those with $W_r(2796) < 0.3 \text{ \AA}$, are related to galaxies similar in type to those associated with “strong” Mg II absorption. There is mounting evidence that a fair number of the weak systems do not arise within ~ 40 kpc of normal, bright galaxies (Churchill & Le Brun 1998; Churchill et al. 1999a).

What are the typical low to high ionization absorption conditions in intermediate redshift Mg II absorption-selected galaxies? Do the majority of Mg II systems have an associated high ionization phase as seen in Si IV, C IV, N V, and O VI absorption? Are there any trends between the high ionization and low ionization absorption strengths? Are there other relationships (or lack of relationships!) that provide clues to the physical nature of galactic gas at intermediate redshifts?

Motivated by these and similar questions, we have under-

¹Based in part on observations obtained at the W. M. Keck Observatory, which is operated as a scientific partnership among Caltech, the University of California, and NASA. The Observatory was made possible by the generous financial support of the W. M. Keck Foundation.

²Based in part on observations obtained with the NASA/ESA *Hubble Space Telescope*, which is operated by the STScI for the Association of Universities for Research in Astronomy, Inc., under NASA contract NAS5-26555.

³Visiting Astronomer at the W. M. Keck Observatory

⁴Center for Gravitational Physics and Geometry

⁵NSF Young Investigator

taken a program to measure the absorption properties of a wide variety of chemical and ionization species associated with Mg II absorbers. Unique to our study is that the Mg II systems have been observed at high resolution ($\sim 6 \text{ km s}^{-1}$) with HIRES/Keck I (Churchill 1997). These spectra also provide a population of weak systems, which are significantly more numerous in their redshift path density (Churchill et al. 1999a). The HIRES spectra cover Mg II, several Fe II transitions, Mg I, and depending upon redshift coverage, Ca II, Ti II, Mn II, and Al III. The remaining absorption properties, including neutral hydrogen and higher ionization species, have been measured in lower resolution ($\sim 230 \text{ km s}^{-1}$) spectra obtained from the *Hubble Space Telescope* archive of the Faint Object Spectrograph.

In this paper, we present the measurements of the absorption lines found in the FOS spectra. Additional analysis focused on the above motivational questions is presented in a parallel companion paper (Churchill et al. 2000, hereafter Paper II). In § 2, we outline our sample selection. Details of the data analysis are presented in § 3. In § 4, we provide a brief description of each system. The general absorption properties are presented in § 5 and a brief synopsis is given in § 6.

2. SAMPLE SELECTION

The Mg II systems for our study were selected from the samples of Steidel & Sargent (1992, hereafter SS92) and Sargent, Boksenberg, & Steidel (1988, hereafter SBS). We obtained HIRES spectra (Vogt et al. 1994) on the Keck I telescope of many of the brightest quasars from the SS92 and SBS database. The optical wavelength coverage for our HIRES spectra translates to a redshift interval of $0.4 \leq z \leq 1.4$ for 28 Mg II systems. An additional 23 systems with equivalent widths below the detection threshold in the SS92 and SBS quasar spectra were discovered in the HIRES spectra, which have a detection threshold of 0.02 \AA (Churchill et al. 1999a). In order to study the wealth of ionization species with transitions further into the ultraviolet, we then searched the *Hubble Space Telescope* archive for Faint Object Spectrograph (FOS) observations of the quasars observed with HIRES/Keck. A number of the FOS spectra were obtained fully reduced from the *HST* QSO Absorption Line Key Project (hereafter KP, Bahcall et al. 1993; Bahcall et al. 1996; Jannuzi et al. 1998). The remaining FOS spectra were obtained from the *HST* archive and reduced using the same methodology as for the KP spectra.

The journal of the HIRES/Keck observations is given in Table 1. The spectral resolution was $R = 45,000$, which corresponds to 6.6 km s^{-1} . From left to right, the columns are the quasar name, the visual magnitude, the emission redshift, the observation date, the total exposure time, and the observed wavelength range. In the continuum near the observed Mg II features, the spectra have signal-to-noise ratios ranging from 15 to 50, with the majority being around 30. The spectra do not have continuous wavelength coverage; there are small gaps redward of 5100 \AA , where the free spectral range of the projected echelle format exceeds the width of the 2048×2048 Tektronix CCD.

There are several FOS observational modes, including grating, polarimetry, and slit settings. We have chosen to limit our survey to the highest resolution spectra ($R = 1300$), obtained with the G130H ($1150\text{--}1600 \text{ \AA}$), G190H ($1600\text{--}2300 \text{ \AA}$) and G270H ($2225\text{--}3275 \text{ \AA}$) gratings. We chose to exclude spectra obtained at lower resolution in order to maintain uniformity and because they are not very useful for narrow-line absorption work.

However, we did use a lower resolution G160L spectrum (in one case) to search for a Lyman limit break. We also opted to exclude spectropolarimetry data because they required additional reduction and calibration steps that did not yield spectra of comparable quality to those obtained with non-spectropolarimetry mode. However, when available, we did use $R = 1300$ spectropolarimetry data to search for Lyman limit breaks and damped Ly α lines at the absorber redshifts. Finally, we excluded spectra with slit widths greater than $1''$. Some of the FOS spectra in our sample were obtained before the COSTAR refurbishing mission. The instrumental spread function of pre-COSTAR spectra introduces broad wings in proportion to the aperture width of the observing mode (Jannuzi & Hartig 1994). We studied only those FOS spectra obtained with fairly narrow apertures in order to mitigate systematics in the absorption line strengths between the pre-COSTAR and COSTAR spectra.

The final selection of FOS spectra are listed in Table 2. From left to right the columns are the quasar name, the alias useful for searching the *HST* archive, the program identification numbers, and the names of the principal investigators for each of the gratings. The observing modes of the KP spectra are described in Jannuzi et al. (1998); the slit widths are all less than $0.26''$. The observing modes of the non-KP spectra vary and are noted in § 4, where each spectrum is individually discussed. We also excluded quasars with complicated broad absorption line features. We make no corrections to these narrow aperture pre-COSTAR spectra and assume a Gaussian instrumental spread function (e.g. Schneider et al. 1993) for measuring equivalent widths in all FOS spectra.

These selection criteria resulted in a sample of 45 Mg II absorbing systems. These systems and their rest-frame equivalent widths are listed in Table 3. The first three columns are the quasar name, the absorber redshift, and the Mg II $\lambda 2796$ rest-frame equivalent width, $W_r(\text{Mg II})$. The remaining columns are explained in § 4. In Figure 1, we show a plot of $W_r(\text{Mg II})$ vs. absorber redshift, z_{abs} . Note that the sample is devoid of $W_r(\text{Mg II}) \geq 0.5 \text{ \AA}$ systems for $z \geq 1$. This is not surprising because the total redshift path above $z \simeq 1$ covered by the HIRES spectra is very small compared to the coverage from $0.4 \leq z \leq 1.0$ and because small equivalent width systems are very common.

The distribution of $W_r(\text{Mg II})$ is shown in Figure 2. Using a maximum likelihood fit (e.g. Lanzetta, Turnshek, & Wolfe 1987), we find that the distribution of our sample follows a power-law with $f(W) \propto W^{-0.9 \pm 0.6}$ for $0.03 \leq W_r(\text{Mg II}) < 1.3 \text{ \AA}$, which is consistent with that of an unbiased sample, $f(W) \propto W^{-1.0 \pm 0.1}$, over this equivalent width range (Churchill et al. 1999a). Between $1.0\text{--}1.3 \text{ \AA}$ the data are systematically below the fit, but are consistent with the maximum likelihood result to 1σ in all bins. Above 1.3 \AA , there is a slight overabundance of systems (not included in the maximum likelihood analysis), due to a selection bias toward larger equivalent width absorbers in the HIRES/Keck survey (Churchill 1997). These are all damped Ly α absorbers. Overall, the sample studied here is consistent with an unbiased sample in its equivalent width distribution for $W_r(\text{Mg II}) < 1.3 \text{ \AA}$ and for $z \leq 1$.

3. DATA ANALYSIS

The HIRES data were processed in the standard manner using the IRAF⁶ *Apextract* package for echelle data. The details of the HIRES data reduction are given in Churchill (1995, 1997). The KP FOS spectra were reduced by the KP collaboration, as described in Schneider et al. (1993), Bahcall et al. (1996), and Jannuzzi et al. (1998). The archival FOS spectra were reduced and calibrated using KP methods.

As a consistency check, we performed two separate, full analyses of the FOS data. The primary analysis invoked *a priori* knowledge of the Mg II redshifts for searching, identifying, and measuring the absorption lines (described in greater detail below). This analysis also used *a priori* knowledge of other metal-line systems along the line of sight (from an exhaustive search of the literature), in order to assess the possibility of misidentifications and blends from these other systems. We developed our own set of automated and graphically interactive software routines for objective feature finding, identifying blending due to other systems, and measuring equivalent widths (including Gaussian deblending). Many of our algorithms are based upon those described by Schneider et al. (1993) and Bahcall et al. (1996). The secondary analysis, which we call the “KP analysis”, was performed as a consistency check. This was an unbiased search for metal-line systems using the KP methodologies (Bahcall et al. 1993; Bahcall et al. 1996; Jannuzzi et al. 1998) and software, i.e. the ZSEARCH and JASON programs. The two full analyses were compared for each FOS absorption line measurement. Though the “KP analysis” yielded different results in detail from those of the primary analysis (i.e. small differences in equivalent widths and their errors), there were very few inconsistencies. In the few cases of differing results, both analyses were studied and a consensus was reached.

3.1. Continuum Fitting

Since the continuum fitting is the most subjective aspect of the data reduction and probably has the most significant impact on the analysis, we briefly elaborate. For the HIRES data, continuum fitting is fairly straight forward because the continuum is well sampled and the signal-to-noise ratio is quite high. We used the technique of Sembach & Savage (1992), which employs Legendre polynomials across a limited regions of spectrum around each of the transitions. The HIRES spectra were not flux calibrated, so the normalized flux is simply relative to the flux levels resulting from the HIRES sensitivity function. Following flux calibration, the FOS spectra were continuum fit as described in Schneider et al. (1993); this entails several iterations of interactive cubic spline fitting to the flux calibrated spectra.

3.1.1. Line Finding

For both the HIRES and the FOS spectra, absorption features were detected using a method slightly modified from that of Schneider et al. (1993), which is optimal in the case of unresolved lines. One constructs a discrete model of the instrumental spread function (ISF) consisting of $M = 2J_0 + 1$ elements, where J_0 is a non-negative integer and $\sum_1^M P_j = 1$. The term P_j is the value at pixel j of a symmetric ISF having a peak value at $j = J_0 + 1$. For both HIRES and FOS, the ISF is modeled as a Gaussian with $R = 45,000$ and 1300 , respectively. We use $J_0 = 6$, which gives a model ISF over 13 pixels.

⁶IRAF is distributed by the National Optical Astronomy Observatories, which are operated by AURA, Inc., under contract to the NSF.

⁷The index k , as written here, provides a minor correction to a previously published version of this formula in Schneider et al. (1993).

The equivalent width of an unresolved feature centered in pixel i is calculated by centering the ISF on the pixel and then computing

$$w(\lambda_i) = \Delta\lambda_i \frac{\sum_{j_1}^{j_2} P_j F(\lambda_k)}{\sum_{j_1}^{j_2} P_j^2}, \quad (1)$$

where $F(\lambda_k) = 1 - I(\lambda_k)/I_c(\lambda_k)$, $I(\lambda_k)$ is the flux in pixel k , $I_c(\lambda_k)$ is its fitted continuum level, $\Delta\lambda_i = (\lambda_{i-1} - \lambda_{i+1})/2$ is the wavelength interval spanned by the pixel, j_1 and j_2 are the minimum and the maximum points in the ISF, and the index⁷ $k = i + (j-1) - J_0$, and where $w(\lambda_i) < 0$ for an absorption feature. At the spectra ends the continuum is extrapolated over J_0 pixels (similar to a wrap around convolution). The uncertainty in $w(\lambda_i)$, is given by

$$\sigma_w(\lambda_i) = \Delta\lambda_i \frac{\left\{ \sum_{j_1}^{j_2} P_j^2 \sigma_F^2(\lambda_k) \right\}^{1/2}}{\sum_{j_1}^{j_2} P_j^2}, \quad (2)$$

where $\sigma_F(\lambda_k) = \sigma_I(\lambda_k)/I_c(\lambda_k)$, and where $\sigma_I(\lambda_k)$ is the 1σ uncertainty in $I(\lambda_k)$ resulting from data reduction and calibration sources and Poisson noise in the quasar flux and sky. This uncertainty “spectrum” serves as the 1σ observed equivalent width detection threshold.

In general terms, an unresolved *absorption* line at pixel i is defined when the pixel equivalent width, $w(\lambda_i)$, is less than $-N\sigma_w(\lambda_i)$, where N is an arbitrarily defined number giving the number of σ beyond the equivalent width detection threshold. For resolved features, the detection is defined over a spectral *region*. The region extremes are defined at the pixels where the $w(\lambda_i)$, which are smooth over the scale length of the ISF, become greater than zero.

For the HIRES spectra, we enforce a 5σ detection threshold. In Figure 3, we show the cumulative distribution of the 5σ rest-frame equivalent width detection threshold of Mg II $\lambda 2796$. Our sample is 100% complete to a 5σ threshold of 0.06 Å, 93% complete to 0.03 Å, and 73% complete to 0.02 Å. For the FOS spectra, we require only a 3σ detection threshold (whereas the “KP analysis” enforced a 4.5σ threshold). We applied a less stringent threshold because we used *a priori* knowledge of the expected location of the absorption lines, whereas the “KP analysis” was an unbiased search for absorption lines, and was therefore more conservative.

3.1.2. Equivalent Widths

For the HIRES spectra, the equivalent widths, W , are measured directly by summing the quantity $[1 - I(\lambda_i)/I_c(\lambda_i)]\Delta\lambda_i$ across the profiles. The measurement uncertainties are obtained from quadrature summing the quantity $\sigma_I(\lambda_i)[\partial W/\partial I(\lambda_i)]$. The equivalent width uncertainties do not account for subjectivity in the continuum placement.

For the FOS spectra, the equivalent widths and their uncertainties were measured by fitting Gaussians to the absorption features. The quoted equivalent widths and uncertainties were taken from our own measurements (i.e. not from the “KP analysis”). We have used an interactive χ^2 minimization scheme, where the minimization is performed by the NETLIB-SLATEC

routine⁸ DNLS1 (More 1978). The uncertainties in the fitted parameters, the Gaussian amplitudes, widths, and centers, are computed using a modified version of the routine DFRIDR (Press et al. 1992). The equivalent width uncertainties are based upon standard error propagation, including correlated terms. For a given line, the minimum allowed Gaussian width is set by the instrumental resolution.

Due to the number density of absorption features and the limited resolution of the FOS spectra, Gaussian deblending was sometimes required. Deblending was used only in cases where the individual line centroids were clearly separated or where a weak blend in the wing of a stronger line showed clear “double” structure. Otherwise, a blend was quoted. Examples of the deblending cases are illustrated in Figure 4, which shows the SiIV doublet at $z = 0.9902$ in PG 1634 + 706; $\lambda 1393$ lies between two Ly α lines and $\lambda 1402$ resides in the wing of Galactic Mg II $\lambda 2796$.

3.1.3. Wavelength Zero Point Shifting of FOS Spectra

The velocity zero points of the KP FOS spectra were defined by setting the mean of the singly ionized transitions from Galactic clouds to redshift zero (see Savage et al. 1993). The archival FOS spectra, on the other hand, were not zero point shifted immediately following their reduction. In both the KP and archival spectra, analysis of the different absorption lines associated with the Mg II systems often revealed a systematic velocity shift with respect to the HIRES spectra, which yielded very precise ($\sigma_z/z \simeq 10^{-6}$), heliocentric, vacuum wavelength, absorption redshifts from Mg II.

We adjusted the zero points of the FOS spectra using a constant velocity shift, which was often determined from the mean velocity offsets of two or more Mg II systems along the line of sight. Since Si II and C II have ionization states similar to Mg II, they were used to derive the shift. If neither Si II nor C II was available, then we used Ly α and/or C IV. The largest shift we applied was no larger than $\sim 70\%$ of a FOS spectral resolution element.

3.1.4. Line Identification Policy in FOS Spectra

Our philosophy for the detection and identification of lines in the crowded FOS spectra is as follows [also see § 4 of Bahcall et al. (1996)]. We generated an objective list of lines using a 3σ detection criterion (see § 3.1.1). This relatively “liberal” threshold was chosen because we are not producing a formal catalog of all absorbers, but have precise redshifts from Mg II in the HIRES spectra. In addition, the continuum fits to the FOS spectra were conservative in that they are probably systematically low in regions of dense line blending.

We examined, case by case, those lines that happen to be coincident with the predicted positions of the transitions from Si, O I, N I, Fe II, Si II, Al II, Si II, C II, Al III, N II, Fe III, Si III, Si IV, Si V, N III, C III, C IV, S VI, N V, O VI, and the Lyman series. For several of the above species, multiple transitions were covered, allowing either examination of a “clean” region of spectrum, or data that corroborated or ruled out identifications in “confused” regions. Some of these transitions were rarely detected at the 3σ level. We did not search regions of the spectra having an observed equivalent width detection threshold greater than 3 Å.

⁸NETLIB is a collection of mathematical software, papers, and databases maintained by AT&T Bell Laboratories, the University of Tennessee, and Oak Ridge National Laboratory (www.netlib.org).

⁹Additional transitions can be consistent if they: a) are not covered, b) have equivalent widths between the scaled $f\lambda$ value and the equivalent width of the strongest transitions, c) are in a blend for which the contribution of the transition of interest could be consistent.

A fair fraction of the time, line blending with transitions from other absorbing systems (some from our sample) was problematic. We attempted to identify all lines involved with blends as follows: We constructed a list of 100 transitions with accurate rest-frame wavelengths (Morton 1991) and a list of all known absorption redshifts, including Ly α “systems” for which Ly β could be confirmed, from an exhaustive literature search (optical and ultraviolet observations) for known systems. In most all cases, a viable candidate for a blend could be determined.

For a given system, a species/transition is identified under the following conditions: 1) there is at least one 3σ detection that can be identified with a transition of the species; 2) all other covered transitions of the species are not inconsistent with the identification⁹; 3) at least one transition is not blended with a possible transition from another system, or, if it is, can be unambiguously deblended using Gaussian fitting (meaning that it is on the wing of a line or has its own clear line center, see § 3.1.2). In the cases of doublets, if the weaker member of a doublet is not inconsistent with the first, then we quote it as a detection. This can occur when the second member is in a blend or is not covered by the spectrum. It is always possible that a doublet is a chance match with two “random” lines, but this type of false match is expected to have small probability in our spectra, based upon the simulations by Bahcall et al. (1996) and by Jannuzi et al. (1998).

If a species was detected in fewer than 10% of the systems, it was eliminated from our overall presentation. Each species has what we call a “flag transition”. The flag transitions are those with the strongest $f\lambda$ for each chemical/ionization species. For the non-doublet transitions, they are Fe II $\lambda 2600$, Mg I $\lambda 2853$, Al II $\lambda 1670$, C II $\lambda 1334$, Si II $\lambda 1260$, and Si III $\lambda 1206$. If the flag transition for the species is not identifiable using the above criteria, but a weaker transition is, the equivalent width of the weaker transition is quoted (in Table 4). We list these for completeness, but do not include them in our analysis.

In spectral regions with no detected absorption lines, the 3σ equivalent width limits were computed from Equation 2, assuming unresolved features. For any given undetected species, the transition with the most stringent limit was adopted. If there was a blend at the expected position of the transition, then an “upper limit” was obtained by quoting the equivalent width of the blended absorption line(s). Due to flat fielding uncertainties, the minimum limit quoted (observer frame) is 0.13 Å (see Bahcall et al. 1996).

3.1.5. Measuring Lyman Limit Breaks

Measurements of the Lyman limit breaks were made using KP techniques, as discussed in Schneider et al. (1993) and Jannuzi et al. (1998). In the cases of multiple or double breaks, we modeled the data employing the same technique applied by Churchill & Charlton (1999; see their Figure 3a). The redshifts of the Lyman limit break models were fixed at the redshifts of the Mg II absorbers. We varied the H I column densities and superimposed synthetic spectra on the data. The quoted optical depths were obtained from the best matching model spectrum. Because the signal-to-noise ratio was often low, we did not use any fitting statistics, but simply attempted to make the depth of the break consistent with the model. In the cases of possible double or multiple breaks (due to redshift proximity), this

modeling technique was successful at either singling out which Mg II system actually gives rise to the break, or placing constraints on the relative strengths of the double break. When a Lyman break is present, we quote a rough estimate of its optical depth in § 4.1, where each absorber is discussed individually. We also place a “+” in column six of Table 4 (described in § 4). If a break was not present, we tabulated a “–” and assign an upper limit on $\log N(\text{H}_1)$ of 16.8 cm^{-2} . When the location of the break was not covered in the spectra, we placed a “...”.

4. PRESENTATION OF SYSTEM PROPERTIES

Line identifications of absorption features in FOS spectra is often plagued by line blending and other sources of confusion. Thus, we believe that a fairly complete description of the issues encountered with each system is warranted, especially in view of the possibility that any single system may be the subject of future detailed study as higher quality data become available.

The results from the HIRES/Keck spectra are presented in Table 3. Tabulated are the quasar name, the absorber redshift, the $\text{Mg II } \lambda 2796$ rest-frame equivalent width, $W_r(\text{Mg II})$, the $\text{Fe II } \lambda 2600$ rest-frame equivalent width, $W_r(\text{Fe II})$, and the $\text{Mg II } \lambda 2853$ rest-frame equivalent width, $W_r(\text{Mg I})$. Equivalent width limits are quoted at the 3σ level. In a few systems, we have detected Mn II , Ca II , or Ti II ; their detection is mostly an arbitrary function of wavelength coverage. We have not listed them in Table 3 (however, we show these data in Figure 5).

In Table 4, we present the results from the FOS/HST spectra. Tabulated are the quasar name, the absorber redshift, the $\text{Ly } \alpha$, $\text{Ly } \beta$, and $\text{Ly } \gamma$ equivalent widths, status of the Lyman break, and the equivalent widths of Al II , Al III , Si II , Si III , Si IV , C II , C III , C IV , N V , and O VI . All equivalent widths are rest frame. The spectroscopic data are presented in Figures 5a–ss. For each system, three sets of panels are shown: the HIRES detections, the FOS detections, and the FOS limits. The spectra are all normalized by the continuum fits. Both pre–COSTAR and COSTAR spectra are represented. We note the pre–COSTAR spectra in the discussion of individual systems (§ 4.1).

The panels with HIRES profiles show a velocity window of -250 to 250 km s^{-1} centered on the $\text{Mg II } \lambda 2796$ optical depth mean. Ticks above the continuum give the velocity positions of the Voigt profiles components (the Voigt profile decomposition is described in Paper II). The panels with singlet FOS absorption lines show a velocity window of -1250 to 1250 km s^{-1} centered on the line. The panels with doublet FOS absorption lines also show a velocity window of -1250 to 1250 km s^{-1} , but the zero point is arbitrarily set half way between the doublet members in order to center the doublet in the panel. Ticks above the FOS spectra show the expected positions of the absorption based upon the Mg II Voigt profile components.

For each system we show the flag transition or both members of a doublet for the species presented in Tables 3 and 4. If a weaker transition was used for a measurement, then it is labeled in Figures 5a–ss and a footnote is placed in Table 3 or Table 4. For the HIRES spectra, we show the strongest Ti II , Ca II , and/or Mn II , even though these species are not listed in Table 3.

4.1. Discussion of the Individual Systems

4.1.1. Q 0002 + 051, UM 18 ($z_{\text{em}} = 1.90$)

The FOS spectra of this quasar, which has four intervening Mg II absorbers, were previously studied by Jannuzzi et al. (1998) and Koratkar et al. (1998). Jannuzzi et al. obtained only

the G270H grating spectrum, with pre–COSTAR optics, and using the $0.25'' \times 2''$ slit. Koratkar et al. obtained both the G190H and G270H grating spectra in spectropolarimetry mode ($1.0''$ aperture). We have included only the Jannuzzi et al. spectrum in our study, except for a constraint on the Lyman limit break obtained from the Koratkar et al. G190H spectrum.

$z = 0.5915$ — This system has no detectable Fe II or Mg I in the HIRES spectrum. In the FOS spectrum, $\text{Si II } \lambda 1526$ is blended with a $\text{Ly } \gamma$ line at $z = 1.5000$ and we thus conservatively fit the entire blend and quote an upper limit for $W_r(\text{Si II})$. $\text{C IV } \lambda 1548$ is blended with $\text{Si II } \lambda 1260$ at $z = 0.9560$ and with $\text{Ly } \gamma$ at $z = 1.5359$. The quoted upper limit for $W_r(\text{C IV})$ is taken to be the 3σ equivalent width limit at the expected position of $\lambda 1550$. $\text{Al II } \lambda 1670$ is blended with $\text{Ly } \delta$ at $z = 1.8016$ so we measure that line and record it as the limit on $W_r(\text{Al II})$. The Lyman limit was not covered.

$z = 0.8514$ — This system is rich in Fe II and Mg I in the HIRES spectrum. In the FOS spectrum, the quoted $W_r(\text{Ly } \alpha)$ may be very slightly overestimated due to the coincidence of $\text{Si III } \lambda 1206$ at $z = 0.8665$. We caution that the $\text{Si II } \lambda 1526$ transition is weak relative to our claimed $\lambda 1260$ detection, but is consistent within the permitted scaling. Jannuzzi et al. (1998) identified a $\text{Ly } \alpha$ line at $z = 1.3592$ at the location of $\text{C IV } \lambda 1548$, but our new knowledge of the presence of a Mg II system implies our preferred $\text{C IV } \lambda 1548$ identification. The unphysical doublet ratio of $\text{C IV } \lambda\lambda 1548, 1550$ is due to a blend of $\lambda 1550$ with $\text{Ly } \beta$ at $z = 1.8016$, which is part of a clear Lyman series. Both members of the $\text{Si IV } \lambda\lambda 1393, 1402$ doublet are blended, the former with $\text{Ly } \beta$ at $z = 1.5160$ and the latter with Galactic $\text{Fe II } \lambda 2586$. A limit on $W_r(\text{Si IV})$ was recorded based on measuring the blend at the expected position of $\text{Si IV } \lambda 1393$. $\text{N V } \lambda 1242$ is blended with $\text{Ly } \beta$ at $z = 1.2472$. There is a strong Lyman limit break with $\tau \simeq 1.4$.

$z = 0.8665$ — This system has no detectable Fe II or Mg I in the HIRES spectrum. In the FOS spectrum, the blue wing of the $\text{Ly } \alpha$ line is blended with $\text{Ly } \delta$ at $z = 1.3866$; we deblended the lines with a Gaussian fit to obtain the quoted $W_r(\text{Ly } \alpha)$. Jannuzzi et al. (1998) favored the identification of a $\text{Ly } \alpha$ line at $z = 1.5653$ at the location of $\text{Al II } \lambda 1670$. Furthermore, the profile is extremely broad (greater than 500 km s^{-1} in the rest-frame), suggesting a blend; we thus quote an upper limit on $W_r(\text{Al II})$. $\text{Si III } \lambda 1206$ is coincident with the strong $\text{Ly } \alpha$ line at $z = 0.8514$. $\text{Si IV } \lambda 1393$ is blended with Galactic $\text{Fe II } \lambda 2600$ so an upper limit on $W_r(\text{Si IV})$ was measured at the position of $\lambda 1402$. $\text{C IV } \lambda 1548$ is blended with $\text{Ly } \beta$ at $z = 1.8184$; we used the 3σ limit on $\lambda 1550$ to compute the upper limit on $W_r(\text{C IV})$. From a model of the Lyman limit, we determined that this system does not contribute to the observed break from the $z = 0.8514$ system.

$z = 0.9560$ — This system has no detectable Fe II or Mg I in the HIRES spectrum. In the FOS spectrum, we claim a detection of $\text{Si III } \lambda 1206$, but note that it could be blended with $\text{Ly } \beta$ at $z = 1.3011$ (if $\text{Ly } \alpha$ is hidden in a complex blend at 2797 \AA). $\text{Si II } \lambda 1260$ is blended with $\text{Ly } \gamma$ at $z = 1.5359$, and other members of that series are cleanly detected. The other Si II transitions are blended

with other possible lines so cannot be used to corroborate or refute a Si II $\lambda 1260$ identification. We quote a limit on Si II from measurement of the blended line at the position of $\lambda 1260$. Si IV $\lambda 1393$ is blended in the red wing of Ly γ at $z = 1.8016$, but a clean upper limit can be derived from the position of Si IV $\lambda 1402$. The region where the Lyman limit is expected exhibits a complex shape, however, there is no apparent break.

4.1.2. Q 0058 + 019, PHL 938 ($z_{\text{em}} = 1.96$)

Only a fairly low signal-to-noise ratio, G190H FOS spectrum was obtained by Rao & Turnshek (1999) using the $1.0''$ aperture. The signal-to-noise ratio is significantly reduced blueward of the Lyman limit break at ~ 2250 Å.

$z = 0.6127$ — This system is a damped Ly α absorber and is seen to have Fe II, Mg I, Mn II, and Ti II absorption in the HIRES spectrum. In the FOS spectrum, the Si IV $\lambda 1393$ transition is clearly detected, though the $\lambda 1402$ could have a contribution from Ly 11 from the strong Lyman series at $z = 1.4638$. The Lyman limit was not covered.

$z = 0.7252$ — This system has Mg I, but no Fe II, in the HIRES spectrum. In the FOS spectrum, the Lyman series lines are somewhat ambiguous [the data are quite noisy such that $W_r(\text{Ly}\beta)$ is greater than $W_r(\text{Ly}\alpha)$]. The O VI $\lambda 1031$ transition is in the red wing of a strong line, possibly Ly β at $z = 0.7337$; we determine an upper limit on $W_r(\text{OVI})$ at the position of $\lambda 1037$. The Lyman limit was not covered.

4.1.3. PG 0117 + 213 ($z_{\text{em}} = 1.50$)

A G270H FOS spectrum of this quasar was previously studied by Jannuzzi et al. (1998) using the $0.3''$ aperture. Koratkar et al. (1998) obtained spectra in the spectropolarimetry mode using both the G190H and G270H gratings ($1.0''$ aperture). We have limited our study to the G270H spectrum from Jannuzzi et al., with the exception of analysis of Lyman limit breaks and of the damped Ly α line in the G190H spectrum. There are five intervening Mg II absorption systems.

$z = 0.5764$ — This system is a damped Ly α absorber (Rao & Turnshek 1995). In the HIRES spectrum, Mg I, Ca II $\lambda 3969$ and several Ti II transition were detected (Ca II $\lambda 3934$ was not covered). Fe II, expected to be very strong, was not covered in the HIRES spectrum. In the FOS spectrum, Fe II $\lambda 1608$ was detected. We quoted $W_r(\text{Si II})$ using $\lambda 1526$, since all other Si II transitions were available only in the spectropolarimetry G190H spectrum. Al II $\lambda 1670$ is strong and could be affected by a blend with a Ly α line; however we note that $W_r(\text{Al II})$ is consistent with a black-bottom Al II profile with the same kinematic spread as Mg II. We point out that the strong damped Ly α line was measured in a G190H spectrum obtained in spectropolarimetry mode. The Lyman limit was not covered.

$z = 0.7291$ — This system has Fe II and Mg I in the HIRES spectrum. We quoted $W_r(\text{Si II})$ using $\lambda 1526$, since all other Si II transitions were available only in the spectropolarimetry G190H spectrum. We identify C II $\lambda 1334$ in this system. The line was previously identified as Ly β

at $z = 1.2501$ by Jannuzzi et al. (1998), however, the ratio $W_r(\text{Ly}\beta)/W_r(\text{Ly}\alpha)$ would be large for the small $W_r(\text{Ly}\alpha)$ in that system and there are no other transitions to corroborate it. Ly α and the Lyman limit were only covered on the spectropolarimetry G190H spectrum, and could not be measured.

$z = 1.0480$ — This system has Fe II and very weak Mg I detected in the HIRES spectrum. In the FOS spectrum, we have quoted a detection for Si III $\lambda 1206$, though we note Jannuzzi et al. (1998) identify this absorption feature as Ly α at $z = 1.0326$. We quote a C II $\lambda 1334$ detection; though Jannuzzi et al. have identified this feature as Fe II $\lambda 1144$ at $z = 1.3868$, their identification is not consistent with the absence of the Fe II $\lambda 2383$ transition in the more sensitive HIRES spectrum. The quoted upper limit for $W_r(\text{Si IV})$ is obtained from $\lambda 1402$ because $\lambda 1393$ is blended with Galactic Mg I. $W_r(\text{CIV})$ is conservatively quoted as an upper limit because both the $\lambda 1548$ and $\lambda 1550$ are detected just below the 3σ level. There is a partial Lyman limit break with $\tau \simeq 0.9$ measured in the G190H spectropolarimetry spectrum.

$z = 1.3250$ — This system has Fe II, Mg I and Al III $\lambda 1863$ in the HIRES spectrum. The C IV doublet is taken from the ground-based spectrum of SS92, which has resolution $R \simeq 860$. In the FOS spectrum, Ly α is coincident with Si III $\lambda 1206$ from the $z = 1.3430$ Mg II system; the quoted $W_r(\text{Ly}\alpha)$ may be larger than the true Ly α absorption strength. Gaussian deblending was used to measure $W_r(\text{Ly}\beta)$ because the blue wing of the Ly β line is blended with Galactic Fe II $\lambda 2383$, but a clear asymmetry is apparent. $W_r(\text{Si IV}) \lambda 1393$ could have a contribution from a blend with Al II $\lambda 1670$ at $z = 0.9400$, but this contribution should be small. The Si IV $\lambda 1402$ is not formally detected, but this is not inconsistent with $\lambda 1393$ due to an uncertain continuum fit near the spectrum edge; we claim a detection for Si IV. Si III $\lambda 1206$ is blended with Galactic Mg II $\lambda 2803$ in its blue wing and possibly with an unidentified line in its red wing; the equivalent width of the full blend was taken as a limit on Si III. The upper limit for $W_r(\text{N V})$ is obtained from the expected position of $\lambda 1242$ because $\lambda 1238$ is blended with Si III $\lambda 1206$ at $z = 1.3868$. Both O VI $\lambda 1031$ and $\lambda 1037$ are blended with other lines, the former with Ly β at $z = 1.3389$, and the latter with O VI $\lambda 1031$, also from $z = 1.3389$. Absorption from O VI might be present in this system, but it cannot be determined, so we quote an upper limit obtained by fitting the weaker blended feature at the position of $\lambda 1037$. The Lyman limit break shows structure suggestive of a “double break”. A model of the Lyman break revealed that both this system and the $z = 1.3430$ system contribute roughly equally, each having $\tau \simeq 0.6$.

$z = 1.3430$ — This system has Fe II and Al III $\lambda\lambda 1854, 1862$ in the HIRES spectrum. The C IV doublet is taken from the ground-based spectrum of SS92, which has resolution $R \simeq 860$ at the position of the doublet. In the FOS spectrum, N V $\lambda 1238$ is blended with Ly α at $z = 1.3868$. We quote a detection of N V based upon $\lambda 1242$, which is blueward of Ly α at $z = 1.3981$. A significant feature was present at the location of Si IV $\lambda 1393$ redward

of the Ly α forest, but $\lambda 1402$ was not covered. We tentatively claim a detection for the SiIV doublet (consistent with our policy on line identifications). SiIII $\lambda 1206$ is coincident with the strong Ly α line associated with the $z = 1.3250$ MgII absorber; we quote the equivalent width of this line as an upper limit on $W_r(\text{SiIII})$. There is a Lyman limit break with $\tau \simeq 1.3$ measured in the G190H spectropolarimetry spectrum. The Lyman limit break shows structure suggestive of a “double break”. Modeling showed that both this system and the $z = 1.3250$ system contribute roughly equally to the break with each having $\tau \simeq 0.6$.

4.1.4. PKS 0454 – 220 ($z_{\text{em}} = 0.53$)

G130H, G190H, and G270H FOS spectra of this quasar were obtained by M. Burbidge (see Cohen et al. (1991)). Of the pre-COSTAR spectra included in our study, these are the only ones obtained with a “large” aperture ($1''$). As such, the quoted equivalent widths may be systematically small; we did not apply any correction factors.

$z = 0.4744$ — This is a near-DLA system (also see Rao et al. 1995); the measured $W_r(\text{Ly}\alpha) = 5.5 \text{ \AA}$ places it on the logarithmic part of the curve of growth with $N(\text{H}\text{I}) \sim 10^{19.5} \text{ cm}^{-2}$. Due to a blend with SiIII $\lambda 1206$ at $z = 0.4833$ in the red wing of the Ly α line, $W_r(\text{Ly}\alpha)$ could be slightly overestimated. Detected in the HIRES spectrum are several FeII transitions, MgI, and CaII $\lambda 3969$ ($\lambda 3934$ was not covered). In the FOS spectrum, the CIV doublet is present on both the G190H and G270H gratings; the equivalent widths of the $\lambda 1548$ transition measured from the two spectra are consistent ($0.93 \pm 0.04 \text{ \AA}$ and $1.09 \pm 0.11 \text{ \AA}$, respectively.) The red wing of CIII is blended with Ly γ at $z = 0.4833$ and an unidentified line, thus a limit is quoted based on a fit to the blend. OVI $\lambda 1031$ is blended with Ly β at $z = 0.4833$ and $\lambda 1037$ is coincident with both the $\lambda 1031$ member of OVI at $z = 0.4833$ and a dominating unidentified line. We conservatively quote an upper limit on $W_r(\text{OVI})$ based on the equivalent width of the blend at the expected position of OVI $\lambda 1031$. Accurate measurement of the $N(\text{H}\text{I})$ optical depth from the Lyman limit is compromised by geocoronal emission; given that this system is a near-DLA, the flux below $\lambda 1345 \text{ \AA}$ should be zero. Modeling showed that the break itself arises from the $z = 0.4833$ system (see below).

$z = 0.4833$ — In the HIRES spectrum, this system has detected FeII, MgI, and CaII $\lambda 3934$ (CaII $\lambda 3969$ was not covered). In the FOS spectrum, CIV was covered by both the G190H and G270H gratings, but the profile shapes and equivalent widths are not consistent (the G190H appears compromised, but the G270H $\lambda 1548$ transition is large relative to $\lambda 1550$); we have quoted the average of the equivalent widths from the two gratings and present the G270H spectrum in Figure 5. Any SiIII $\lambda 1206$ that is present in the spectrum is blended in the red wing of the Ly α line at $z = 0.4744$; we have quoted $W_r(\text{Ly}\alpha)$ for the upper limit on $W_r(\text{SiIII})$. The upper limit on $W_r(\text{SiIV})$ was obtained from $\lambda 1402$, since $\lambda 1393$ is blended with SiIV $\lambda 1402$ at $z = 0.4744$. OVI $\lambda 1031$ is blended with OVI $\lambda 1037$ at $z = 0.4744$ and a dominating unidentified line. However, a clean upper limit on

$W_r(\text{OVI})$ was obtained from $\lambda 1037$. Modeling showed that the Lyman limit break arises from this system, however accurate measurement of the $N(\text{H}\text{I})$ optical depth is compromised by geocoronal emission.

4.1.5. PKS 0454 + 039 ($z_{\text{em}} = 1.35$)

G190H and G270H FOS spectra of this quasar (obtained by Bergeron with the $1.0''$ square aperture) were studied by Boissé et al. (1998), and a separate G270H spectrum ($1.0''$ round aperture) was obtained by Bowen. We independently reduced these data, and we present results below from the Bergeron G190H and from a combined G270H spectrum from the Bowen and Bergeron observations. Some slight differences between our analysis results and those of Boissé et al. are discussed on a system by system basis below.

$z = 0.6428$ — This system has FeII in the HIRES spectrum. In the FOS spectrum, Ly α is blended with Ly γ at $z = 1.1532$ and a Ly α line at $z = 0.6448$, but it is distinct such that accurate deblending is possible. We claim a tentative detection of SiIV, which appears to be present in both the G190H and G270H spectra. We note however, that the blue wing of $\lambda 1393$ is blended with Ly α at $z = 0.8801$ and that there may be a small contribution to $\lambda 1402$ from Nv $\lambda 1242$ at $z = 0.8596$, though the latter is not formally detected. Though Churchill & Le Brun (1998) claimed a tentative upper limit on CIV, our reduction and continuum fit of the G190H spectrum yielded a detection above the 3σ level; we thus claim a detection for CIV. SiIII $\lambda 1206$ is blended with Ly β at $z = 1.1532$; we fit this feature to obtain an upper limit. The Lyman limit was not covered and Ly β is below the Lyman break from the $z = 0.8596$ system where the flux is zero.

$z = 0.8596$ — This is a well studied damped Ly α system (e.g. Steidel et al. 1995; Lu et al. 1996b; Boissé et al. 1998). In the HIRES spectrum, a suite of five FeII transitions are detected, as are the MnII $\lambda 2600$ triplet, MgI and TiII $\lambda 3074$ and $\lambda 3243$. In the FOS spectrum, numerous transitions are detected, and the optical depth of the Lyman limit is $\tau \simeq 3.3$.

$z = 0.9315$ — This system has FeII in the HIRES spectrum. Our measurement of the very weak Ly α line was consistent with that reported by Churchill & Le Brun (1998). Ly β is blended with the Lyman series at $z = 1.1532$ and Ly γ is blended with Ly δ at $z = 0.9780$. SiIII $\lambda 1206$ is in the blue wing of a Ly α line at $z = 0.9185$ so a non-restrictive limit was obtained by fitting this blend. Though it appears that a clean CIV doublet is present, $\lambda 1548$ is actually FeII $\lambda 1608$ from the $z = 0.8596$ DLA and $\lambda 1550$ is MgII $\lambda 2796$ from a dwarf galaxy at $z = 0.0714$. A non-restrictive limit on $W_r(\text{CIV})$ is obtained by fitting the feature coincident with the expected position of $\lambda 1548$. OVI $\lambda 1031$ is blended with the blue wing of Ly β at $z = 1.1532$ and $\lambda 1037$ is blended with Ly δ , also at $z = 1.1532$; we used $W_r(\text{Ly}\beta)$ to obtain an upper limit on $W_r(\text{OVI})$. There is no Lyman limit break.

$z = 1.1532$ — In the HIRES spectrum, FeII, MgI and the AlIII $\lambda\lambda 1854, 1862$ are present. The CIV doublet is taken from the ground-based spectrum of SBS, which has resolution $R \simeq 2200$ at the observed wavelength of CIV. In the FOS spectrum, the quoted $W_r(\text{SiIV})$ is taken

from $\lambda 1402$ because $\lambda 1393$ is blended with Mg II $\lambda 2796$ from the dwarf galaxy at $z = 0.0714$. Boissé et al. (1998) reported detection of N V $\lambda\lambda 1238, 1242$, but the feature located where $\lambda 1238$ is expected may be a Ly α line at $z = 1.1941$, since $\lambda 1242$ would be in the extreme blue wing of the possible Ly α line at $z = 1.2025$. We quote an upper limit on $W_r(\text{N V})$ from measuring the blend at the position of $\lambda 1238$. Though O VI may be present, $\lambda 1031$ is blended with Ly β at $z = 1.1672$ and O VI is in a complex region in the wing of the damped Ly α line at $z = 0.8596$. The optical depth of the Lyman limit is $\tau \simeq 1.1$.

4.1.6. PKS 0823 – 223 ($z_{\text{em}} > 0.92$)

This quasar, a luminous BL Lacertae object, has only a lower limit on its emission redshift. Only a G270H FOS spectrum was obtained by Rao & Turnshek (1999) using the $1.0''$ aperture.

$z = 0.7055$ — This system has no detectable Fe II or Mg I in the HIRES spectrum. Ly α was not covered in the FOS spectrum. The upper limit on $W_r(\text{Si II})$ is obtained from the $\lambda 1526$ transition because the other Si II transitions are not covered. C II $\lambda 1334$, if present, is blended with strong Si II $\lambda 1190$ at $z = 0.9110$, so this blend is fit to obtain an upper limit on $W_r(\text{C IV})$. For the upper limit on $W_r(\text{Si IV})$, we use $\lambda 1402$ because $\lambda 1393$ is blended with Galactic Fe II $\lambda 2374$ and $\lambda 2383$. The Lyman limit was not covered.

$z = 0.9110$ — This system was reported to be a “double” system by Veron-Cetty et al. (1990). Several Fe II transitions and Mg I are present in the HIRES spectrum. The FOS spectrum is very rich in many, cleanly identified, transitions. The $\lambda 1242$ member of the N V doublet is blended with Galactic Fe II $\lambda 2374$, but $\lambda 1238$ is unambiguously detected. The Lyman break was not covered.

4.1.7. Q 0958 + 551, MRK 132 ($z_{\text{em}} = 1.76$)

The G270H FOS spectrum, obtained with the $0.3''$ round aperture, was studied by Jannuzzi et al. (1998). The FOS spectrum covers only the Ly α forest down to a strong Lyman limit break at 2200 \AA from a $z = 1.7327$ system that wipes out all flux below this wavelength.

$z = 1.2113$ — This system has no detectable Fe II or Mg I in the HIRES spectrum. In the FOS spectrum, Ly α is blended with $\lambda 1550$ from a possible C IV doublet at $z = 0.7330$. There are no corroborating transitions for the C IV redshift in the HIRES spectrum, but there is a possible Fe II $\lambda 1608$ line in the FOS spectrum. We quote a non-restrictive upper limit on $W_r(\text{Ly } \alpha)$. Si III $\lambda 1206$ is blended with C III $\lambda 977$ at $z = 1.7325$, the redshift of the strong Lyman limit break. There is a strong absorption feature coincident with Si II $\lambda 1260$ (could be Fe II $\lambda 1608$ at $z = 0.7330$), but its strength is not consistent with detection limits based to the Si II $\lambda\lambda 1190, 1193$; we have used $\lambda 1193$ to place an upper limit on $W_r(\text{Si II})$. The Lyman limit break was not covered.

$z = 1.2724$ — This system has Fe II $\lambda 2383$ in the HIRES spectrum. The C IV doublet is taken from the ground-based spectrum of SBS, which has resolution $R \simeq 840$ at this wavelength. In the FOS spectrum, only Ly α is

clearly detected above the 3σ threshold. A possible detection of Si IV is not clear; there could be coincident Ly α lines blended with both members of the doublet. We conservatively quote an upper limit on $W_r(\text{Si IV})$. The Lyman limit break was not covered. N V $\lambda 1242$ is possibly blended with O VI $\lambda 1031$ at $z = 1.7327$, so $\lambda 1238$ provides an upper limit on $W_r(\text{N V})$.

4.1.8. PG 1206 + 459 ($z_{\text{em}} = 1.16$)

Both the G190H and G270H FOS spectra of this quasar have been studied by Jannuzzi et al. (1998). They were obtained with pre-COSTAR optics using the $0.25'' \times 2''$ slit. The metal line properties of the Mg II systems were studied in detail by Churchill & Charlton (1999).

$z = 0.9276$ — This system was reported as a double system by Jannuzzi et al. (1998) and by Churchill & Charlton (1999), with redshifts $z = 0.9254$ and $z = 0.9276$. In the HIRES spectrum, Fe II and Mg I are present. The FOS spectrum has the richest complement of transitions of all the systems in our sample. C II $\lambda 1334$ is blended with a possible Ly α line at $z = 1.1166$. C II $\lambda 1036$ is blended with O VI $\lambda 1037$ and with O VI $\lambda 1031$ at $z = 0.9343$. The quoted $W_r(\text{C II})$ is based upon $\lambda 1334$ using a Gaussian deblending, which likely yielded a slightly large value. The C IV profile required a double Gaussian fit and the $\lambda 1550$ from $z = 0.9254$ is blended with $\lambda 1548$ from $z = 0.9276$. We approximately measured $W_r(\text{C IV})$ (estimated uncertainty of $\sim 1 \text{ \AA}$) as the sum of half of the equivalent width of this blend and the equivalent width of the unblended $\lambda 1548$ from the $z = 0.9254$ system. O VI also required a double Gaussian fit, but $W_r(\text{O VI})$ could be determined more accurately due to the larger separation of O VI $\lambda\lambda 1031, 1037$. C III $\lambda 977$ is clearly detected but is blended with Ly α at $z = 0.5482$ and a smaller Ly γ line from the $z = 0.9343$ Mg II absorber; our upper limit is the equivalent width of the blend. Modeling of the Lyman limit showed that the break is entirely due to the $z = 0.9276$ system with $\tau \simeq 0.9$ [see Churchill & Charlton (1999)].

$z = 0.9343$ — This system has no detectable Fe II or Mg I in the HIRES spectrum. $W_r(\text{O VI})$ was measured using $\lambda 1037$ because $\lambda 1031$ is blended with O VI $\lambda 1037$ at $z = 0.9276$. In the FOS spectrum, Ly γ is blended with Ly α at $z = 0.5482$ and C III $\lambda 977$ at $z = 0.9276$ such that only a non-restrictive limit can be derived from a fit to the blend. C II $\lambda 1334$ is blended with strong Ly α at $z = 1.1223$. This system makes no contribution to the Lyman limit break (see notes on the $z = 0.9276$ system).

4.1.9. PG 1241 + 176 ($z_{\text{em}} = 1.27$)

The pre-COSTAR G270H FOS spectrum of this quasar, obtained with the $0.25'' \times 2''$ slit, has been studied by Jannuzzi et al. (1998).

$z = 0.5505$ — In the HIRES spectrum, Fe II, Mg I and Ca II $\lambda 3969$ were detected ($\lambda 3934$ was not covered). In the FOS spectrum, detected Si II $\lambda 1526$ was used to measure $W_r(\text{Si II})$ because no other Si II transitions are covered. The Lyman limit was not covered.

$z = 0.5584$ — This system has no detectable Fe II or Mg I in the HIRES spectrum. In the FOS spectrum, Si II $\lambda 1526$ was used to measure $W_r(\text{Si II})$ because no other Si II transitions are covered. C IV $\lambda 1550$ was not detected at the 3σ level, however, it is consistent with the weak, but significant $\lambda 1548$ detection; we have quoted a detection for C IV. The Lyman limit was not covered.

$z = 0.8955$ — This system has no detectable Fe II or Mg I in the HIRES spectrum. In the FOS spectrum, only Ly α was unambiguously detected. Si III $\lambda 1206$ is blended with O VI $\lambda 1031$ at $z = 1.2154$; it is difficult to evaluate the relative contributions so we quote an upper limit on $W_r(\text{Si III})$. The Si IV doublet is somewhat ambiguous; if real, it is offset redward from the predicted location. The $\lambda 1393$ transition may be Ly α at $z = 1.1742$ and the $\lambda 1402$ transition is blended with C II $\lambda 1334$ at $z = 0.9927$, a system with other corroborating lines. The limit on $W_r(\text{Si IV})$ was determined by fitting the blend at the expected position of $\lambda 1393$. The location of N V $\lambda 1242$ is blended with an unknown transition in the blue wing of O VI $\lambda 1037$ at $z = 1.2720$, but a clean limit on $W_r(\text{N V})$ is determined at the position of $\lambda 1393$. (C II $\lambda 1036$ at $z = 1.2720$ is ruled out as the blend based upon the absence of stronger C II $\lambda 1334$). The Lyman limit was not covered.

4.1.10. PG 1248 + 401 ($z_{\text{em}} = 1.03$)

Both the G190H and G270H FOS spectra ($0.3''$ aperture) of this quasar have been studied by Jannuzi et al. (1998).

$z = 0.7730$ — This system has detected Fe II and Mg I in the HIRES spectrum. The FOS spectrum is very rich with clearly detected transitions. As seen in Ly α and Ly β , there is a higher redshift system at $z = 0.7760$ with no detectable Mg II in the HIRES spectrum. There are no detected metal lines from that system that might contaminate those of the $z = 0.7730$ Mg II absorber. $W_r(\text{Si II})$ was obtained by Gaussian deblending of $\lambda 1260$ with Si III $\lambda 1206$ at $z = 0.8546$. We have tentatively claimed N V as a detection, noting that $\lambda 1242$ is not formally detected, but is consistent with the expected value from $\lambda 1238$. N V was also detected by the systematic procedures of Jannuzi et al. (1998). $W_r(\text{Ly } \gamma)$ is quoted as an upper limit, since its measured value is inconsistent with $W_r(\text{Ly } \alpha)$ and $W_r(\text{Ly } \beta)$. The Lyman limit is on the edge of the G190H spectrum where the signal-to-noise ratio is hopeless.

$z = 0.8546$ — This system has several Fe II transitions but no Mg I in the HIRES spectrum. In the FOS spectrum, this system is part of a group of Ly α + Ly β absorbers at redshifts 0.8524, 0.8585, and 0.8614. This is one of the examples in the KP data set of extensive metal-line systems occurring in overdensities in the distribution of Ly α absorbers (Bahcall et al. 1996; Jannuzi 1998). The blend in the blue wing of Si III $\lambda 1206$ is Si II $\lambda 1260$ at $z = 0.7730$. $W_r(\text{Si III})$ was obtained by Gaussian deblending. We quote an upper limit on $W_r(\text{Si IV})$ because $\lambda 1393$ is blended with Galactic Fe II $\lambda 2586$ and $\lambda 1402$ is blended with Galactic Fe II $\lambda 2600$. There is no Lyman limit break in a very clean portion of the spectrum.

4.1.11. Q 1317 + 277, TON 153 ($z_{\text{em}} = 1.02$)

Both the G190H and G270H FOS spectra of this quasar have been studied by Bahcall et al. (1996). These spectrum were obtained with pre-COSTAR optics using the $0.25'' \times 2''$ slit. The G160L FOS spectrum, covering the Lyman limit, was presented by Bahcall et al. (1993).

$z = 0.6601$ — In the HIRES spectrum, Fe II, Mg I are present. In the FOS spectrum, there is an unknown blend with N V $\lambda 1242$ but a clean upper limit on $W_r(\text{N V})$ is taken from the position of $\lambda 1238$. O VI $\lambda 1031$ is blended with Ly β at $z = 0.6691$; we used $\lambda 1037$ to place an upper limit on $W_r(\text{O VI})$. There is a strong Lyman limit break, with $\tau \simeq 5.4$, associated with this system.

4.1.12. PG 1329 + 412 ($z_{\text{em}} = 1.94$)

The G190H grating spectrum ($1.0''$ aperture) was obtained by K. Lanzetta. The G270H grating was obtained by Rao & Turnshek (1999), also with the $1.0''$ aperture. This is a complex spectrum with at least 10 known metal-line absorption redshifts, several of which give rise to a Lyman series. In the G190H spectrum, there is a strong Lyman limit break at 2083 \AA from a $z = 1.2841$ system that wipes out all flux below this wavelength. The two strongest Lyman series systems at $z = 1.8408$ and $z = 1.8367$, give rise to a partial Lyman limit break. The former is associated with a C IV absorber (SBS) and has strong O VI $\lambda\lambda 1031, 1037$ absorption in the FOS spectrum.

$z = 0.5008$ — This system had no detectable Fe II nor Mg I in the HIRES spectrum. In the FOS spectrum, the upper limit on $W_r(\text{Si II})$ was obtained using the $\lambda 1526$ transition since it was the only Si II line redward of the strong Lyman limit break at $z = 1.2841$. The Si IV $\lambda\lambda 1393, 1402$ is sitting on the shoulder of this break, and is thus fairly noisy, with $\lambda 1402$ blended with a possible Ly α line at $z = 0.7308$; a non-restrictive upper limit is quoted from the noisy region at the expected position of $\lambda 1393$. The Lyman limit was not covered.

$z = 0.8933$ — The HIRES spectrum is relatively noisy so that some weak kinematic outlying clouds could be missed. Near Mg II $\lambda 2796$ there is an unidentified line at $v = +80 \text{ km s}^{-1}$ (which cannot be Mg II because the $\lambda 2803$ transition is absent). Fe II was detected, but Mg I was not present. In the FOS spectrum, only Ly α is detected. Al II $\lambda 1670$ is blended in the red wing of strong Ly α at $z = 1.6008$. C II $\lambda 1334$ is blended with Ly δ , also at $z = 1.6008$. The Si IV doublet is on the shoulder of the “double”, partial Lyman limit break systems; $\lambda 1393$ is blended with Ly δ at $z = 1.8336$ and $\lambda 1402$ is blended with the blue wing of a complex blend, including two Ly ϵ lines at $z = 1.8366$ and 1.8408 , and Ly β at $z = 1.6008$. We quote an upper limit for $W_r(\text{Si IV})$. The upper limit on $W_r(\text{C IV})$ is obtained using $\lambda 1550$ because $\lambda 1548$ is blended with O VI $\lambda 1031$ at $z = 1.8408$. The Lyman limit is wiped out by the break at 2083 \AA .

$z = 0.9739$ — This system has no detectable Fe II transitions nor Mg I in the HIRES spectrum. In the FOS spectrum, the Ly α line is the central member of a triple blend with Ly γ at $z = 1.4716$ being the red-most member and an unidentified line (possibly Ly α at $z = 0.9729$) to the blue. The quoted $W_r(\text{Ly } \alpha)$ was obtained by Gaussian

deblending, but because the profile is complicated the error is likely underestimated. $W_r(\text{SiII})$ was also obtained using Gaussian deblending, due to an unidentified line, possibly Ly α at $z = 1.0499$. The CII $\lambda 1334$ transition is detected in a crowded region of the spectrum, but is unblended between Ly6 at $z = 1.8366$ and Ly7 at $z = 1.8408$. SiIV $\lambda 1393$ is clearly detected, not being blended with any Lyman series lines, however, $\lambda 1402$ is blended with Ly α at $z = 1.2830$, which is corroborated by a Ly β line. For CIV, $\lambda 1550$ is stronger at the 4σ level, suggesting a blend. The upper limit on $W_r(\text{Nv})$ is obtained from $\lambda 1242$ because $\lambda 1238$ is blended with NIII $\lambda 989$ at $z = 1.4714$. The Lyman limit is wiped out by the break at 2083 Å.

$z = 0.9984$ — This system has several FeII transitions, but MgI was not covered in the HIRES spectrum. In the FOS spectrum, the Ly α is blended with an unidentified line; we measured $W_r(\text{Ly}\alpha)$ using Gaussian deblending, but note that the value is uncertain. CII is blended with a strong Ly α line at $z = 1.6008$. SiIV $\lambda 1402$ is blended with Galactic MgII $\lambda 2803$. The CIV doublet, which brackets a possible Ly α line at $z = 1.5477$, is undetected. There is also a possible Ly α line at $z = 1.0371$ slightly to the blue of Nv $\lambda 1238$. The Lyman limit is wiped out by the break at 2083 Å.

4.1.13. PKS 1354 + 195 ($z_{\text{em}} = 0.72$)

The G160L, G190H, and G270H FOS spectra of this quasar have been studied by Jannuzzi et al. (1998) and Bergeron et al. (1994). These spectra were obtained pre-COSTAR, using the $0.25'' \times 2''$ slit.

$z = 0.4566$ — The HIRES spectrum is fairly noisy in the region of the MgII doublet and FeII transitions, so it is possible that some kinematic outlying clouds were missed. FeII $\lambda 2600$ and MgI were detected. In the FOS spectrum, the detections are all unambiguous and the upper limits are not compromised by blends. We note that there is a Lyman limit break with $\tau \simeq 0.9$ in the G160L spectrum (Jannuzzi et al. 1998).

$z = 0.5215$ — This system has no detected FeII transitions nor MgI in the HIRES spectrum. SiIII $\lambda 1206$ is blended with SiII $\lambda 1260$ at $z = 0.4566$, that latter being corroborated by the presence of a proper-strength SiII $\lambda 1526$ line. The line at the expected wavelength of CII $\lambda 1334$ is SiIV $\lambda 1393$ at $z = 0.4566$. Based upon the G160L spectrum, there is no evidence for a Lyman limit break at this redshift.

4.1.14. Q 1622 + 238, 3C 336 ($z_{\text{em}} = 0.93$)

Both the G190H and G270H FOS spectra ($1.0''$ aperture) of this quasar have been studied by Steidel et al. (1997). The background level for the G190H is not certain. The spectrum has slightly negative flux in the core of the damped Ly α line at $z = 0.6561$ and below the Lyman limit break. Thus, the equivalent widths of lines measured in this grating may be systematically small. The HIRES spectrum is quite noisy, such that the detection threshold is low for accompanying transitions.

$z = 0.4720$ — In the HIRES spectrum, only the MgII doublet is detected. In the FOS spectrum, the CIV $\lambda 1550$ is

blended with SiIII $\lambda 1206$ at $z = 0.8913$, but the $\lambda 1548$ appears to be clear. The upper limit on $W_r(\text{SiII})$ was obtained from $\lambda 1526$ on the G270H grating because the stronger $\lambda 1260$ transition was in a noisy region of the G190H spectrum. CII is ambiguous, being in a very noisy part of the spectrum and possibly being blended with OVI $\lambda 1037$ at $z = 0.8913$; we quote the 3σ upper limit on $W_r(\text{CII})$. The upper limit on $W_r(\text{SiIV})$ is obtained using $\lambda 1402$ because $\lambda 1393$ is blended with a strong line, which could be Ly α at $z = 0.6868$ with a contribution from Nv $\lambda 1238$ at $z = 0.6561$. The Lyman limit break was not covered.

$z = 0.6561$ — This system is a damped Ly α absorber (Steidel et al. 1997). In the HIRES spectrum, FeII is strong and TiII $\lambda 3385$ is detected. In the FOS spectrum, the upper limit on $W_r(\text{Nv})$ is obtained using $\lambda 1242$ because $\lambda 1238$ is blended with a strong line, which could be Ly α at $z = 0.6868$ with a contribution from SiIV $\lambda 1393$ at $z = 0.4720$. The Lyman limit break was not covered.

$z = 0.7971$ — This system was first seen in CIV absorption. Only the MgII $\lambda 2803$ transition was detected because $\lambda 2796$ was wiped out by the pen mark on the HIRES CCD. Neither FeII nor MgI was detected. SiIV $\lambda 1402$ is blended with CII $\lambda 1334$, but $\lambda 1393$ is cleanly measured. A robust measurement of $W_r(\text{Ly}\beta)$ was not possible due to the signal to noise of the spectrum. Also, Ly β may suffer from blending so we have quoted an upper limit on $W_r(\text{Ly}\beta)$. Though SiIII $\lambda 1206$ is in a busy part of the FOS spectrum, there are no other candidates for the line; the line immediately to the blue is FeII $\lambda 1145$ at $z = 0.8913$. The OVI was not formally detected in a noisy region of the spectrum. The region of the spectrum corresponding to the Lyman limit is very noisy due to the break at $z = 0.8913$.

$z = 0.8913$ — In this system, FeII, MgI, and MnII $\lambda 2577$ and $\lambda 2594$ were detected in the HIRES spectrum. In the FOS spectrum, SiII $\lambda 1260$ is blended with Galactic FeII $\lambda 2383$, so the $\lambda 1193$ transition of the $\lambda 1190, 1193$ doublet is used to measure $W_r(\text{SiII})$. $W_r(\text{CII})$ was measured using Gaussian deblending, where the blue wing is SiIV $\lambda 1402$ at $z = 0.7971$. Nv $\lambda 1238$ is blended with Galactic FeII $\lambda 2344$; we obtained the limit on $W_r(\text{Nv})$ using $\lambda 1242$. The OVI doublet is ambiguous, being in a very noisy part of the spectrum and possibly being blended with CII $\lambda 1334$ at $z = 0.4720$; we quote a limit on $W_r(\text{OVI})$. There is a Lyman limit break with a large optical depth whose accurate measurement is difficult.

4.1.15. PG 1634 + 706 ($z_{\text{em}} = 1.34$)

The G270H FOS spectrum of this quasar were studied by (Bahcall et al. 1996). This spectrum was taken with the pre-COSTAR optics using a $0.25'' \times 2''$ slit. A pre-COSTAR spectropolarimetry G190H spectrum was obtained with the wide, $4.3''$ by Impey et al. (1996). We did not include the G190H spectrum in our study except to investigate the Lyman limit breaks.

$z = 0.8182$ — This system has no detected FeII transitions nor MgI in the HIRES spectrum. There were no detection in the FOS spectrum. The upper limit on $W_r(\text{SiII})$ is

taken from $\text{SiII } \lambda 1526$, which provided the best limit despite being blended with $\text{SiIV } \lambda 1393$ at $z = 0.9902$. The apparent, but slightly offset, $\text{AlII } \lambda 1670$ is $\text{SiII } \lambda 1526$ at $z = 0.9902$, as corroborated by $\text{SiII } \lambda 1260$. The upper limit on $W_r(\text{SiIV})$ is fairly clean, given the density of lines near the $\lambda 1393$ transition; $\lambda 1402$ is likely a blend, possibly with a $\text{Ly}\alpha$ line at $z = 1.0984$. There is no flux at the position of the Lyman limit due to the strong break from the $z = 0.9902$ system.

$z = 0.9056$ — This system has no detected FeII transitions nor MgI in the HIRES spectrum. In the FOS spectrum, the upper limit on $W_r(\text{SiII})$ is obtained using $\lambda 1193$ because $\lambda 1260$ is coincident with $\text{SiIII } \lambda 1206$ at $z = 0.9902$. $\text{CII } \lambda 1334$ may be present, but the observed equivalent width is $0.11 \pm 0.04 \text{ \AA}$, which is below the suggested threshold of 0.13 \AA for a detection limit in order to avoid flat fielding residuals in the reduced spectrum (Bahcall et al. 1996). (The signal-to-noise ratio of this spectrum is higher than many of the available flat fields for the epoch of these observations of PG 1634 + 706.) $\text{SiIV } \lambda 1393$ is coincident with $\text{CII } \lambda 1334$ at $z = 0.9902$; we obtained $W_r(\text{SiIV})$ using $\lambda 1402$, which lies in the extended red wing of a possible $\text{Ly}\alpha$ line at $z = 1.1979$. The $\text{Nv } \lambda 1238$ line includes a contribution from $\text{SiII } \lambda 1190$ at $z = 0.9902$. This implies that the candidate $\lambda 1238$ line is unrealistically strong relative to $\lambda 1242$, and also the separation of the centroids of the two lines do not agree. We measure $W_r(\text{Nv})$ for the candidate $\lambda 1238$ line, but cautiously quote this value only as an upper limit. There is no flux at the position of the Lyman limit due to the strong break from the $z = 0.9902$ system.

$z = 0.9902$ — In the HIRES spectrum, this system has several detected FeII transitions and detected MgI . In the FOS spectrum, there is a $\text{Ly}\alpha$ line at $z = 0.9785$ in the red wing of $\text{SiIII } \lambda 1206$; $W_r(\text{SiIII})$ was obtained using Gaussian deblending. Both members of the SiIV doublet are blended, but easily modeled with Gaussian fitting. The $\lambda 1393$ transition is the central member of a three line blend with $\text{Ly}\alpha$ at $z = 1.2788$ and $z = 1.2852$ and the $\lambda 1393$ transition is in the blue wing of Galactic $\text{MgII } \lambda 2796$ (see Figure 4). The feature just blueward of where $\text{Nv } \lambda 1238$ is expected is $\text{SiIII } \lambda 1206$ at $z = 1.0414$; a 3σ limit was determined at the expected position of $\lambda 1242$. There is a strong Lyman limit break with $\tau > 6.0$ that wipes out all flux blueward of 1815 \AA .

$z = 1.0414$ — This system has no detected FeII transitions nor MgI in the HIRES spectrum. In the FOS spectrum, the detections are without ambiguity, except perhaps $\text{CII } \lambda 1334$, which could be an artifact of flat fielding problems. The relatively strong feature between $\text{SiIV } \lambda 1393$ and $\lambda 1402$ is Galactic MgI . $\text{Nv } \lambda 1242$ is blended with $\text{Ly}\alpha$ at $z = 1.0881$, but a 3σ limit was measured at the position of $\lambda 1238$. There is a Lyman limit break with $\tau \simeq 1.4$.

4.1.16. PKS 2128 – 123, PHL 1598 ($z_{\text{em}} = 0.50$)

Both the G190H and G270H FOS spectra of this quasar have been studied by Jannuzi et al. (1998). The optics were pre-COSTAR and a $0.25'' \times 2''$ slit was used.

$z = 0.4297$ — This system is a near-DLA, with $W_r(\text{Ly}\alpha) = 2.92 \text{ \AA}$. In the HIRES spectrum, FeII was

not covered, whereas MgI and both members of the $\text{CaII } \lambda\lambda 3934, 3969$ were detected. In the FOS spectrum, there is no confusion with $\text{Ly}\alpha$ absorbers due to the low redshift of the quasar. We quote a detection for the SiIV doublet, since $\lambda 1393$ is detected and $\lambda 1402$ is consistent with its expected strength (recall that there is no $\text{Ly}\alpha$ forest confusion, nor are there any other metal-line systems). We obtained an upper limit (albeit not very constraining) on $W_r(\text{FeII})$ using $\lambda 1145$. The Lyman limit was not covered.

4.1.17. PKS 2145 + 067 ($z_{\text{em}} = 1.00$)

Both the G190H and G270H FOS spectra of this quasar have been studied by Bahcall et al. (1993) and by Bergeron et al. (1994). These were obtained with pre-COSTAR optics using the $0.25'' \times 2''$ slit.

$z = 0.7908$ — In the HIRES spectrum, FeII was detected, but MgI was not. From the FOS spectrum, we quote a detection for $\text{SiII } \lambda 1260$ based upon its correct strength relative to detected $\text{SiII } \lambda 1193$, although we note Bahcall et al. (1996) identified the line as $\text{Ly}\alpha$ at $z = 0.8577$. The line to the red of $\text{SiIII } \lambda 1206$ is $\text{Ly}\alpha$ at $z = 0.7810$, which has a corroborating $\text{Ly}\beta$ line, thus this is not a doublet at another redshift, and a SiIII detection is claimed. Nv is detected, but we note that $\lambda 1242$ is probably blended with another absorption feature. $\text{CII } \lambda 1334$ is not detected at 3σ , which means that the strong feature to the blue of $\text{OVI } \lambda 1037$ is not $\text{CII } \lambda 1036$; it is likely $\text{Ly}\alpha$ at $z = 0.5266$. The Lyman limit is located in an extremely noisy region of the G190H spectrum and no measurement is possible. See Bergeron et al. (1994) for an independent study of the FOS data for this system.

5. OVERALL ABSORPTION PROPERTIES

For most systems, the measured absorption properties are not without some ambiguity in one transition or another. We do not anticipate that highly detailed system by system analyses can be made. That is not to say that, in some cases where robust measurements of extreme properties are measured, physical information cannot be extracted [e.g. the absorbers toward PG 1206 + 459 (Churchill & Charlton 1999)]. However, we are confident that our analysis of the data has yielded measurements that provide a sound representation of the absorption properties of the sample as a whole, given the consistency between our two independent methods for identifying absorption lines (see § 3). Here, we present the general overall properties of the systems and discuss a few of the more immediately obvious trends in the data. We reserve further analysis for Paper II.

In Figure -10, we present the rest-frame absorption strengths of the species listed in Tables 3 and 4 vs. that of MgII . Only the “flag transitions” are plotted. If a transition other than the “flag transition” was used to measure an equivalent width or an upper limit on an equivalent width, the value was not plotted on any of the figures. However, this results in a negligible difference to the general appearance of Figure -10. For all data, the median errors are roughly the size of the data points and those points with downward pointing arrows represent upper limits. Though there are very few $\text{CaII } \lambda\lambda 3934, 3969$ data points (due to redshift coverage), we have presented CaII absorption strengths for

comparison with the numerous studies focused on the Galaxy, and on local and low redshift galaxies (e.g. Morton & Blades 1986; Robertson et al. 1988; Bowen 1991a, 1999b; Vallerga et al. 1993; Sembach, Danks, & Savage 1993; Welty, Morton, & Hobbs 1996).

Spearman-Kendall non-parametric rank correlation tests, including upper limits (Isobe, Feigelson, & Nelson 1986; LaValley, Isobe, & Feigelson 1992), show that the absorption strengths of all transitions with ionization potentials less than that of CII (~ 25 eV) are correlated with $W_r(\text{Mg II})$ at a greater than 97% confidence level (with the exception of CaII). We take this as additional confirmation that our measurements, for the most part, provide an accurate representation of the overall sample, since it is expected that these absorption strengths should be correlated. Note, however, that since most of the low ionization transitions are saturated, their equivalent widths are a better measure of the overall kinematic spread of the gas than of column densities (e.g. Petitjean & Bergeron 1990, 1994). An interesting trend with ionization level is that, as $W_r(\text{Mg II})$ is increased above 1 Å, the low ionization strengths correspondingly increase whereas the higher ionization strengths have considerable scatter and a relatively low mean. Most of the latter data represent the damped Ly α systems, as can be seen by their large $W_r(\text{Ly } \alpha)$ values. Accurate measurements of N V and O VI were fairly rare, but from the few data points available, it would appear that $W_r(\text{N V})$ is often less than 0.4 Å, and that O VI may have a range of absorption strengths similar to CIV.

Based upon photoionization models (Bergeron & Stasińska 1986; SS92), it has been widely accepted that Mg II absorbers are optically thick at the Lyman limit in neutral hydrogen, i.e. they have neutral hydrogen column densities of $N(\text{H I}) \geq 2 \times 10^{17} \text{ cm}^{-2}$ in one or more of the kinematic components. In Figure -9, we present the rest-frame equivalent widths of Mg II and CIV vs. that of Ly α . Three data point types are shown. Those systems with a measured Lyman limit break are solid circles, those with no break are open circles, and those for which the break was not covered are open squares. The majority of Mg II absorbers have Ly α strengths in the rough range 0.5–2 Å, with a sparsely populated tail extending out to ~ 10 Å. It is not clear if there is a gap in the distribution of $W_r(\text{Ly } \alpha)$; this would occur if damped Ly α systems [by definition those with $N(\text{H I}) \geq 2 \times 10^{20} \text{ cm}^{-2}$, which corresponds to $W_r(\text{Ly } \alpha) \geq 9$ Å] are more common than are "H I rich" systems with $W_r(\text{Ly } \alpha)$ in the intermediate range ~ 2 –8 Å. Since these H I-rich, but non-damped, systems have strong Mg II absorption (most above 0.6 Å), their co-moving number density probably evolves in close step with the strongest Mg II absorbers (SS92).

The Ly α transition is easily saturated and is thus not a good measure of the neutral hydrogen column density. The Lyman limit break can provide an estimate of $N(\text{H I})$ and is the unambiguous signature of optically thick neutral hydrogen (Tytler 1982). The location of Lyman limit break was covered for 17 of the 45 absorbers. All but two of the systems with $W_r(\text{Ly } \alpha) > 1$ Å have breaks; it is likely that nearly all metal-line systems in this equivalent width range would also have breaks (also see Jannuzi et al. 1998).

Since the redshift number density of the weakest Mg II systems is several times greater than that of systems with Lyman limit breaks (Churchill et al. 1999a), it is expected that most Mg II absorbers with $W_r(\text{Mg II}) < 0.3$ Å will not have a break. We find two weak systems with breaks, six without, and nine

undetermined. We note that the majority of the systems have $W_r(\text{Ly } \alpha) \leq 1.0$ Å, and none of these for which the location of the Lyman limit was covered has a break. This suggests, not surprisingly, that the weakest of the weak Mg II absorbers are the ones lacking breaks. Note that the presence of a Lyman break is independent of CIV strength in that the full range of observed $W_r(\text{CIV})$ exhibit breaks. Also, note that the CIV strengths are relatively small in the damped Ly α systems, implying that their CIV kinematics are probably similar to a more "typical" strong Mg II absorber.

In Figure -8, we present the rest-frame equivalent widths of SiIV and CII vs. that of CIV. As with Figure -10, we plot "flag transitions" only. In the plot of $W_r(\text{CII})$ vs. $W_r(\text{CIV})$, we illustrate the combined effects of a range of kinematics and ionization conditions. We also present $W_r(\text{SiIV})$ vs. $W_r(\text{CIV})$, which has been central for studying the ionization conditions in the ISM and Halo of the Galaxy (e.g. Savage, Sembach, & Lu 1997). Future high resolution spectra of these particular transitions will be essential for a detailed understanding of the kinematics and ionization conditions of the ISM and halos of these intermediate redshift galaxies.

For future detailed studies using higher resolution data, silicon has the added virtue of sampling three ionization states. Thus, we also present the rest-frame equivalent widths of Si III vs. Si II, and of Si III and Si II vs. SiIV, in Figure -7. Again, we plot "flag transitions" only. Since both silicon and magnesium are α -process elements, and Si II and Mg II have nearly identical ionization potentials and transitions with similar oscillator strengths, it is expected that Si II will tightly trace Mg II. The Si III $\lambda 1206$ transition, however, is very strong and is expected to be saturated, even at high resolution.

It is evident that the relative kinematics between the low and high ionization phases vary from absorber to absorber as seen in Figures -8 and -7. For equivalent widths greater than ~ 0.4 Å there is a large range of values (lack of correlations) for CII and SiIV vs. CIV and for Si II and Si III vs. SiIV.

6. CONCLUSION

We have measured the absorption properties of 45 intermediate redshift Mg II absorbers in FOS spectra from the *HST* archive and from the database of the *HST* QSO Absorption Line Key Project. The sample was selected from the 51 Mg II systems observed with HIRES/Keck for which FOS spectra of the same quasars existed. The Mg II profiles, and other transitions observed in the optical, have been resolved at $\sim 6 \text{ km s}^{-1}$ resolution. The UV FOS spectra have resolution $\sim 230 \text{ km s}^{-1}$. In this paper, we presented the data, the data analysis, and a brief description of the properties of each system. We present additional analysis of the data in a parallel companion paper (Paper II).

We have found evidence for a high ionization gaseous phase in intermediate redshift Mg II absorbing galaxies. Mostly, the high ionization species detected are CIV and SiIV, which are commonly seen in absorption in the Galaxy (e.g. Savage & Sembach 1996; Savage, Sembach, & Lu 1997). These data lead us to suggest that these galaxies have multiphase interstellar media and halos similar to those observed locally (Dahlem 1998; also see Churchill et al. 1999b).

What is the kinematic spread of the CIV and what is its line of sight velocity structure? How is this structure related to that seen in Mg II? High resolution spectroscopic observation are sorely needed for sorting out the physical nature of this high ionization material and its relation to the kinematically complex

low ionization gas. Only if the high ionization profiles are resolved at resolutions comparable to the HIRES/Keck data, can the *relative* kinematics of the low and high ionization gas can be quantified.

Support for this work was provided by the NSF (AST-9617185), and NASA (NAG 5-6399 and AR-07983.01-96A)

the latter from the Space Telescope Science Institute, which is operated by AURA, Inc., under NASA contract NAS5-26555. BTJ acknowledges support from NOAO, which is operated by AURA, Inc., under cooperative agreement with the NSF. We thank Blair Savage for providing a table of Galactic absorption properties in electronic form.

REFERENCES

Bahcall, J. L., and Spitzer, L. Jr. 1969, *ApJ*, 156, L63
 Bahcall, J. N., et al. . 1993, *ApJS*, 87, 1
 Bahcall, J. N., et al. . 1996, *ApJ*, 457, 19
 Bergeron, J., et al. 1994, *ApJ*, 436, 33
 Bergeron, J., & Boissé, P. 1991, *A&A*, 243, 344
 Bergeron, J. and Stasińska, G. 1986, *A&A*, 169, 1
 Boissé, P., Le Brun, V., Bergeron, J., Deharveng, J.-M. 1998, *A&A*, 333, 841
 Bowen, D. V. 1991a, *MNRAS*, 145, 649
 Bowen, D. V. 1991b, *MNRAS*, 251, 649
 Charlton, J. C., & Churchill, C. W. 1998, *ApJ*, 499, 181
 Churchill, C. W. 1995, Lick Technical Report, 74
 Churchill, C. W. 1997, Ph.D. Thesis, University of California, Santa Cruz
 Churchill, C. W., & Charlton, J. C. 1999, *AJ*, 118, 59
 Churchill, C. W. & Le Brun, V. 1998, *ApJ*, 499, 677
 Churchill, C. W., Mellon, R. R., Charlton, J. C., Jannuzzi, B. T., Kirhakos, S., Steidel, C. C., & Schneider, D. P. 1999b, *ApJ*, 519, L43
 Churchill, C. W., Mellon, R. R., Charlton, J. C., Jannuzzi, B. T., Kirhakos, S., Steidel, C. C., & Schneider, D. P. 2000, *ApJ*, submitted (Paper II)
 Churchill, C. W., Rigby, J. R., Charlton, J. C., & Vogt, S. S. 1999a, *ApJS*, 120, 51
 Churchill, C. W., Steidel, C. C., & Vogt, S. S. 1996, *ApJ*, 471, 164
 Cohen, R. D. Bartko, F., Beaver, E. A., Burbidge, E. M., Junkharinen, V. T., Lyons, R. W., Rosenblatt, E. I., Burks, G. S.; Harma, R. J., & Henriksen, M. 1991, *BAAS*, 23, 1426
 Dahlem, M. 1998, *PASP*, 110, 1298
 Guillemin, P., & Bergeron, J. 1997, *A&A*, 328, 499
 Impey, C., Petry, C. E., Malkan, M. A., & Webb, W. 1996, *ApJ*, 463, 473
 Isobe, T. Feigelson, E. D., & Nelson, P. I. 1986, *ApJ*, 306, 490
 Jannuzzi, B. T. 1998, in *Structure and Evolution of the IGM from QSO Absorption Line Systems*, eds. P. Petitjean & S. Charlot, (Paris : Editions Frontieres), 93
 Jannuzzi, B. T., et al. 1998, *ApJS*, 118, 1
 Jannuzzi, B. T., & Hartig, G. F. 1994, in *Calibration of the Science Instruments on HST*, ed. J. C. Blades & S. Osmer (Baltimore : STScI), 215
 Koratkar, A., Antonucci, R., Goodrich, R. & Storrs, A. 1998, *ApJ*, 503, 599
 LaValley, M., Isobe, T., & Feigelson, E. 1992, in *Astronomical Data Analysis Software and Systems I*, ASP Conf. Series, V25, D.M. Worrall, C. Biemesderfer, & J. Barnes, eds., 245
 Lanzetta, K. M., Turnshek, D. A., & Wolfe, A. M. 1987, *ApJ*, 322, 739
 Lu, L., Sargent, W. L. W., Barlow, T. A., Churchill, C. W., & Vogt, S. S. 1996, *ApJS*, 107, 475
 More, J. J. 1978, in *Numerical Analysis Proceedings*, ed. G.A. Watson, Lecture Notes in Mathematics (Garching : Springer-Verlag), 630
 Morton, D. C., & Blades, J. C. 1986, *MNRAS*, 220, 927
 Morton, D. C. 1991, *ApJS*, 77, 119
 Petitjean, P., & Bergeron, J. 1990, *A&A*, 231, 309
 Petitjean, P., & Bergeron, J. 1994, *A&A*, 283, 759
 Press, W. H., Flannery, B. P., Teukolsky, S. A., & Vetterling, W. T. 1992, *Numerical Recipes*, (Cambridge : Cambridge University Press)
 Rao, S. M., & Turnshek, D. A. 1995, *ApJ*, 499, 488
 Rao, S. M., & Turnshek, D. A. 1999, in preparation
 Robertson, J. G., Morton, D. C., Blades, J. C., York, D. G., & Meyer, D. M. 1988, *ApJ*, 325, 635
 Sargent, W. L. W., Boksenberg, A., & Steidel, C. C. 1988, *ApJS*, 68, 539 (SBS)
 Savage, B. D., et al. 1993, *ApJ*, 413, 116
 Savage, B. D., & Sembach, K. R. 1996, *ARA&A*, 34, 279
 Savage, B. D., Sembach, K. R., & Lu, L. 1997, *AJ*, 113, 2158
 Schneider et al. 1993, *ApJS*, 87, 45
 Sembach, K. R., Danks, A. C., & Savage, B. D. 1993, *A&AS*, 100, 107
 Sembach, K. R., & Savage, B. D. 1992, *ApJS*, 83, 147
 Steidel, C. C. 1995, in *QSO Absorption Lines*, ed. G. Meylan (Garching : Springer Verlag), 139
 Steidel, C. C., Bowen, D. V., Blades, J., & Dickinson, M. 1995, *ApJL*, 440, 45
 Steidel, C. C., Dickinson, M., Meyer, D. M., Adelberger, K. L., & Sembach, K. R. 1997, *ApJ*, 480, 568
 Steidel, C. C., Dickinson, M. & Persson, E. 1994, *ApJ*, 437, L75
 Steidel, C. C., & Sargent, W. L. W. 1992, *ApJS*, 80, 1 (SS92)
 Tytler, D. 1982, *Nature*, 298, 427
 Tytler, D., Boksenberg, A., Sargent, W. L. W., Young, P., & Kunth, D. 1987, *ApJS*, 64, 667
 Vallerga, J. V., Vedder, P. W., Craig, N., & Welsh, B. Y. 1993, *ApJ*, 411, 729
 Veron-Cetty, M.-P., Djorgovski, S., Magain, P., Meylan, G., & Surdjen, J., *A&A Supp*, 86, 543
 Vogt, S. S., et al. 1994, in *Proceedings of the SPIE*, 2128, 326
 Welty, D. E., Morton, D. C., & Hobbs, L. M. 1996, *ApJS*, 106, 533
 Yanny, B. 1992, *PASP*, 104, 840
 Yanny, B., and York, D. G. 1992, *ApJ*, 391, 569

TABLE 1
JOURNAL OF HIRES/KECK OBSERVATIONS

QSO	V [mag]	z_{em}	Date [UT]	Exp [s]	λ Range [Å]
0002 + 051	16.2	1.90	1994 Jul 5	2700	3655.7–6079.0
0058 + 019	17.2	1.96	1996 Jul 18	3000	3766.2–5791.3
0117 + 213	16.1	1.50	1995 Jan 23	5400	4317.7–6775.1
0454 – 220	15.5	0.53	1995 Jan 22	5400	3765.8–6198.9
0454 + 039	16.5	1.35	1995 Jan 22	4500	3765.8–6198.9
0823 – 223	15.7	> 0.92	1995 Jan 24	3600	3977.8–6411.8
0958 + 551	16.0	1.76	1995 Jan 23	3600	5400.0–7830.0
1206 + 459	16.1	1.16	1995 Jan 23	3600	3810.5–6304.9
1241 + 176	15.4	1.27	1995 Jan 22	2400	3765.8–6189.9
1248 + 401	16.3	1.03	1995 Jan 22	4200	3765.8–6189.9
1317 + 277	16.0	1.02	1995 Jan 23	3600	3810.5–6304.9
1329 + 412	16.3	1.94	1996 Jul 18	6300	3766.2–5791.3
1354 + 195	16.0	0.72	1995 Jan 22	3600	3765.8–6189.9
1622 + 238	18.3	0.93	1994 Jul 4,5	16,200	3726.9–6191.0
1634 + 706	14.9	1.34	1994 Jul 4,5	2700	3723.3–6185.7
2128 – 123	15.9	0.50	1996 Jul 19	3900	3766.2–5791.3
2145 + 067	16.3	1.00	1996 Jul 18	4500	3766.2–5791.3

TABLE 2
FOS ARCHIVAL DATA USED FOR THIS STUDY

QSO	Alias	Program ID and PI		
		G130H (1150–1600 Å)	G190H (1600–2300 Å)	G270H (2225–3275 Å)
0002 + 051	UM 18	...	6705(Koratkar)	4581(KP)
0058 + 019	PHL 938	...	6577(Rao)	...
0117 + 213	PG	...	6109(Koratkar)*	5664(KP)
0454 – 220	PKS	1026(Burbidge)	1026(Burbidge)	1026(Burbidge)
0454 + 039	PKS	...	5351(Bergeron)	5351(Bergeron)+5451(Bowen)
0823 – 223	PKS	6577(Rao)
0958 + 551	MRK 132	5664(KP)
1206 + 459	PG	...	2424(KP)	2424(KP)
1241 + 176	PG	4112(KP)
1248 + 401	PG	...	5664(KP)	5664(KP)
1317 + 277	TON 153	...	2424(KP)	2424(KP)
1329 + 412	PG	...	5948(Lanzetta)	6577(Rao)
1354 + 195	PKS	...	2424(KP)	2424(KP)
1622 + 238	3C 336	...	5304(Steidel)	5304(Steidel)
1634 + 706	PG	...	3732(Impey)*	3221(KP)
2128 – 123	PKS, PHL 1598	...	4581(KP)	4581(KP)
2145 + 067	PKS	...	2424(KP)	2424(KP)

* Spectropolarimetry mode; limited use (see text).

Note:— KP indicates the observation was either part of the QSO Absorption Line Key Project (PI J. Bahcall) observations or from the GTO observations of J. Bahcall.

TABLE 3
DATABASE AND HIRES/KECK RESULTS^a

QSO	z_{abs}	$W_r(\text{Mg II}) [\text{\AA}]$	$W_r(\text{Fe II}) [\text{\AA}]$	$W_r(\text{Mg I}) [\text{\AA}]$
0002 + 051	0.5915	0.103 \pm 0.008	< 0.012	< 0.010
	0.8514	1.086 \pm 0.016	0.419 \pm 0.022	0.166 \pm 0.027
	0.8665	0.023 \pm 0.008	< 0.010	< 0.007
	0.9560	0.052 \pm 0.007	< 0.005	< 0.005
0058 + 019	0.6127	1.625 \pm 0.013	1.274 \pm 0.037	0.300 \pm 0.062
	0.7252	0.253 \pm 0.012	< 0.034	0.041 \pm 0.026
0117 + 213	0.5764	0.906 \pm 0.100	0.270 \pm 0.050 ^b	0.155 \pm 0.023
	0.7291	0.238 \pm 0.009	0.075 \pm 0.016	0.013 \pm 0.009
	1.0480	0.415 \pm 0.009	0.065 \pm 0.010	0.027 \pm 0.011
	1.3250	0.291 \pm 0.011	0.026 \pm 0.009	0.005 \pm 0.002
	1.3430	0.153 \pm 0.008 ^b	0.029 \pm 0.004 ^b	< 0.010
0454 - 220	0.4744	1.382 \pm 0.009	0.975 \pm 0.029	0.333 \pm 0.014
	0.4833	0.431 \pm 0.007	0.162 \pm 0.043	0.070 \pm 0.010
0454 + 039	0.6428	0.118 \pm 0.008	0.037 \pm 0.014	< 0.005
	0.8596	1.445 \pm 0.014	1.232 \pm 0.014	0.306 \pm 0.022
	0.9315	0.042 \pm 0.005	0.030 \pm 0.008 ^b	< 0.005
	1.1532	0.432 \pm 0.012	0.084 \pm 0.015	0.026 \pm 0.012
	0823 - 223	0.7055	0.092 \pm 0.007	< 0.008
0958 + 551	0.9110	1.276 \pm 0.016	0.416 \pm 0.026	0.224 \pm 0.031
	1.2113	0.060 \pm 0.007	< 0.006	< 0.010
	1.2724	0.081 \pm 0.007	0.017 \pm 0.004	0.007 \pm 0.002
1206 + 459	0.9276	0.878 \pm 0.016	0.077 \pm 0.020	0.042 \pm 0.020
	0.9343	0.049 \pm 0.005	< 0.004	< 0.004
1241 + 176	0.5505	0.481 \pm 0.019	0.236 \pm 0.048	0.098 \pm 0.030
	0.5584	0.135 \pm 0.014	< 0.012	< 0.008
	0.8955	0.018 \pm 0.005	< 0.005	< 0.004
1248 + 401	0.7730	0.694 \pm 0.009	0.247 \pm 0.020	0.065 \pm 0.022
	0.8546	0.235 \pm 0.014	0.031 \pm 0.007	< 0.019
1317 + 277	0.6601	0.338 \pm 0.011	0.126 \pm 0.016	0.026 \pm 0.009
	1329 + 412	0.5008	0.258 \pm 0.035	< 0.100
1354 + 195	0.8933	0.400 \pm 0.023	0.080 \pm 0.035	< 0.055
	0.9739	0.181 \pm 0.035	< 0.028	< 0.024
	0.9984	0.142 \pm 0.010	0.058 \pm 0.017	...
	0.5215	0.030 \pm 0.007	< 0.012	< 0.007
	1622 + 238	0.4720	0.681 \pm 0.048	< 0.118
1634 + 706	0.6561	1.449 \pm 0.029	1.015 \pm 0.050	0.291 \pm 0.027
	0.7971	0.274 \pm 0.029	< 0.092	< 0.254
	0.8913	1.534 \pm 0.025	1.080 \pm 0.421	0.307 \pm 0.033
	0.9056	0.064 \pm 0.004	< 0.005	< 0.004
	0.9902	0.558 \pm 0.005	0.127 \pm 0.011	0.058 \pm 0.010
2128 - 123	1.0414	0.097 \pm 0.008	< 0.038	< 0.003
	0.4297	0.406 \pm 0.014	< 0.260 ^b	0.162 \pm 0.026
2145 + 067	0.7908	0.483 \pm 0.015	0.041 \pm 0.014	< 0.038

^a All equivalent widths are rest-frame and their limits are 3σ .

^b Not “flag” transition; see system notes (§3)

TABLE 4
FOS/HST RESULTS^a

QSO	z_{abs}	$W_r(\text{Ly}\alpha)$	$W_r(\text{Ly}\beta)$	$W_r(\text{Ly}\gamma)$	Ly lim	$W_r(\text{AlII})$	$W_r(\text{AlIII})$	$W_r(\text{SiII})$	$W_r(\text{SiIV})$	$W_r(\text{CII})$	$W_r(\text{CIII})$	$W_r(\text{CIV})$	$W_r(\text{Nv})$	$W_r(\text{OVI})$		
0002 + 051	0.5915	< 0.70	< 0.11	< 0.30 ^b	< 0.23 ^b		
	0.8514	2.47 ± 0.08	+	0.25 ± 0.05	...	0.66 ± 0.09	1.15 ± 0.11	< 0.82	0.54 ± 0.06	...	1.26 ± 0.06	< 0.15		
	0.8665	0.81 ± 0.10	-	< 0.66	...	< 0.12	< 2.45	< 0.11 ^b	< 0.12	...	< 0.11 ^b	< 0.18		
	0.9560	0.85 ± 0.07	-	< 0.15	...	< 0.61	0.32 ± 0.07	< 0.10 ^b	< 0.10	...	0.52 ± 0.04	< 0.12		
	0.6127	6.77 ± 0.40	1.22 ± 0.45	0.76 ± 0.14	0.64 ± 0.18	0.51 ± 0.11	0.74 ± 0.12	< 0.36	< 0.71	
0058 + 019	0.7252	0.46 ± 0.13	0.75 ± 0.19	< 0.30	< 0.27	...	< 0.18	< 0.85	...	< 0.30	< 0.40 ^b	
	0.5764	11.15 ± 1.09	0.96 ± 0.04	< 0.11	0.33 ± 0.05 ^b	0.58 ± 0.06		
	0.7291	< 0.10	< 0.12 ^a	< 0.10 ^b	...	< 0.12	0.23 ± 0.06	...	< 0.10	...		
	1.0480	1.93 ± 0.04	+	< 0.08	0.44 ± 0.04	< 0.09 ^b	0.31 ± 0.07	...	< 0.08	< 0.07		
	1.3250	1.51 ± 0.03	0.30 ± 0.04	...	+	< 0.07	< 0.30	0.33 ± 0.04	0.19 ± 0.03	0.65 ± 0.05	0.89 ± 0.03	< 0.08 ^b	< 0.19 ^b	
0454 - 220	1.3430	1.19 ± 0.04	0.70 ± 0.03	0.64 ± 0.05	+	0.21 ± 0.03	< 1.49	0.26 ± 0.04	0.17 ± 0.03	0.57 ± 0.04	0.67 ± 0.02	0.17 ± 0.03 ^b	0.18 ± 0.03	
	0.4744	3.74 ± 0.05	0.96 ± 0.07	0.86 ± 0.08	...	0.61 ± 0.05	0.16 ± 0.05	0.51 ± 0.02	0.67 ± 0.04	0.45 ± 0.03	0.76 ± 0.03	< 1.59	0.63 ± 0.03	< 0.06	< 0.75	
	0.4833	1.56 ± 0.03	0.74 ± 0.07	< 1.58	+	0.13 ± 0.06	< 0.11	0.12 ± 0.02	< 3.60	< 0.07 ^b	0.53 ± 0.04	0.43 ± 0.07	0.38 ± 0.11	< 0.14	< 0.84	
	0.6428	0.70 ± 0.05	-	< 0.10	< 0.11	< 0.13	< 0.49	0.29 ± 0.10	< 0.11	...	0.46 ± 0.05	< 0.12	...	
	0.8596	10.70 ± 0.26	2.36 ± 0.13	2.26 ± 0.04	+	0.69 ± 0.04	...	0.89 ± 0.05	0.75 ± 0.03	0.70 ± 0.04	0.77 ± 0.04	1.39 ± 0.11	0.66 ± 0.03	< 0.17 ^b	0.58 ± 0.11	
0454 + 039	0.9315	0.17 ± 0.04	< 0.41	< 0.95	-	< 0.09	...	< 0.10	< 0.65	< 0.09	0.18 ± 0.03	< 0.17	< 0.46	< 0.08	< 0.49	
	1.1532	1.61 ± 0.03	1.63 ± 0.03	1.26 ± 0.03	+	0.34 ± 0.03	1.09 ± 0.05	0.27 ± 0.05 ^b	0.38 ± 0.03	0.92 ± 0.03	0.94 ± 0.06	< 0.46	< 1.18	
	0823 - 223	0.7055	< 0.13	< 0.12 ^a	< 0.13 ^b	...	< 0.16 ^b	< 1.37	...	< 0.18	
	0.9110	2.68 ± 0.07	0.31 ± 0.05	...	0.91 ± 0.07	1.34 ± 0.06	0.44 ± 0.06	1.50 ± 0.06	...	1.34 ± 0.06	0.18 ± 0.06	...	
	0958 + 551	< 0.92	< 0.23 ^b	< 2.15	< 0.24	< 0.24	< 0.23	...	
1206 + 459	1.2113	< 0.23	< 0.22	< 0.24	< 0.24	...	0.44 ± 0.03	< 0.22	...	
	1.2724	0.75 ± 0.15	0.61 ± 0.07	1.06 ± 0.09	0.64 ± 0.06	0.84 ± 0.05	< 2.22	1.84 ± 0.52	1.00 ± 0.16	1.32 ± 0.06	
	0.9276	2.47 ± 0.07	1.70 ± 0.05	1.41 ± 0.06	+	< 0.15	< 0.13	< 0.15	< 0.10	< 0.84	0.24 ± 0.04	0.25 ± 0.05	< 0.12 ^b	0.11 ± 0.04 ^b
	0.9343	0.47 ± 0.07	0.30 ± 0.04	< 2.29	-	< 0.15	< 0.13	< 0.15	< 0.10	< 0.84	
	1.241 + 176	0.5505	0.22 ± 0.07	< 0.10	0.37 ± 0.06 ^b	0.83 ± 0.07	
1248 + 401	0.5584	< 0.11	< 0.12	< 0.37 ^b	0.21 ± 0.06	
	0.8955	0.45 ± 0.05	< 0.10	...	< 0.10	< 0.40	< 0.27	< 0.10	...	< 0.10	< 0.08	...	
	0.7730	1.45 ± 0.04	0.82 ± 0.06	< 1.25	...	0.16 ± 0.06	...	0.29 ± 0.03	0.65 ± 0.03	0.30 ± 0.03	0.25 ± 0.06	0.37 ± 0.08	0.65 ± 0.06	0.12 ± 0.03	0.23 ± 0.05	
	0.8546	1.46 ± 0.29	1.06 ± 0.04	0.69 ± 0.05	-	< 0.12	...	< 0.09	1.04 ± 0.04	< 0.13 ^b	0.23 ± 0.03	0.54 ± 0.04	0.68 ± 0.06	0.40 ± 0.12	0.34 ± 0.05	
	1317 + 277	0.6601	1.48 ± 0.03	0.84 ± 0.05	...	+	< 0.14	< 0.14	0.43 ± 0.03	0.42 ± 0.04	< 0.15	0.22 ± 0.04	0.66 ± 0.14	< 0.14	< 0.07	< 0.13 ^b
1329 + 412	0.5008	< 0.22	< 0.16	< 0.41 ^b	...	< 0.96	< 0.40	
	0.8933	1.15 ± 0.16	< 3.17	...	< 0.25	< 0.34	< 0.47	< 1.81	...	< 0.12 ^b	< 0.32	...	
	0.9739	1.15 ± 0.23	0.17 ± 0.08	0.53 ± 0.10	0.66 ± 0.05	0.23 ± 0.06	...	0.87 ± 0.05	< 0.17 ^b	...	
	0.9984	0.31 ± 0.20	< 0.16	< 0.19	< 0.12	< 0.73	...	< 0.11	< 0.18	...	
	1354 + 195	0.4566	1.72 ± 0.08	...	+	< 0.24	< 0.17	0.39 ± 0.07	0.42 ± 0.08	0.56 ± 0.08	0.78 ± 0.10	...	0.91 ± 0.04	< 0.17	...	
1622 + 238	0.5215	1.08 ± 0.08	-	< 0.22	< 0.19	< 0.18	< 0.37	< 0.09	< 0.53	...	< 0.24	< 0.17	...	
	0.4720	1.27 ± 0.27	< 0.20	...	< 0.28 ^b	< 0.67	< 0.48 ^b	< 0.56	...	0.46 ± 0.14	< 0.62	...	
	0.6561	9.42 ± 0.34	0.53 ± 0.07	< 0.16	1.00 ± 0.16	1.06 ± 0.13	0.16 ± 0.07	0.64 ± 0.13	...	0.29 ± 0.09	< 0.43 ^b	...	
	0.7971	1.38 ± 0.14	< 1.63	< 0.10	...	< 0.23	0.61 ± 0.16	0.48 ± 0.07	0.40 ± 0.06	...	1.25 ± 0.06	< 0.29	< 0.65	
	0.8913	2.98 ± 0.10	1.08 ± 0.20	< 0.58	+	0.50 ± 0.05	...	0.44 ± 0.08 ^b	0.96 ± 0.07	0.70 ± 0.07	0.71 ± 0.09	1.21 ± 0.20	0.82 ± 0.05	< 0.08 ^b	< 0.44	
1634 + 706	0.8182	< 0.16	...	< 0.35 ^b	...	< 0.07	< 0.07	...	< 0.07	
	0.9056	0.49 ± 0.03	< 0.07	...	< 0.07 ^b	0.11 ± 0.02	< 0.12 ^b	< 0.07	...	0.18 ± 0.02	< 0.38	...	
	0.9902	1.09 ± 0.03	+	0.25 ± 0.02	0.39 ± 0.03	0.32 ± 0.03	0.38 ± 0.02	...	0.32 ± 0.02	< 0.07	...	
	1.0414	1.42 ± 0.01	+	< 0.06	0.43 ± 0.03	0.26 ± 0.01	0.10 ± 0.01	...	0.40 ± 0.02	< 0.06	...	
	2128 - 123	0.4297	2.92 ± 0.08	0.31 ± 0.09	< 0.33	0.26 ± 0.04	0.27 ± 0.08	0.20 ± 0.05	0.37 ± 0.05	...	0.40 ± 0.04	< 0.17	...	
2145 + 067	0.7908	1.22 ± 0.04	0.79 ± 0.07	0.77 ± 0.09	...	< 0.20	...	0.40 ± 0.06	0.84 ± 0.04	0.41 ± 0.07	< 0.27	0.84 ± 0.07	1.13 ± 0.08	0.30 ± 0.08	0.83 ± 0.11	
	

^a All equivalent widths are rest-frame and their limits are 3σ .

^b Not “flag” transition; see system notes (§3).

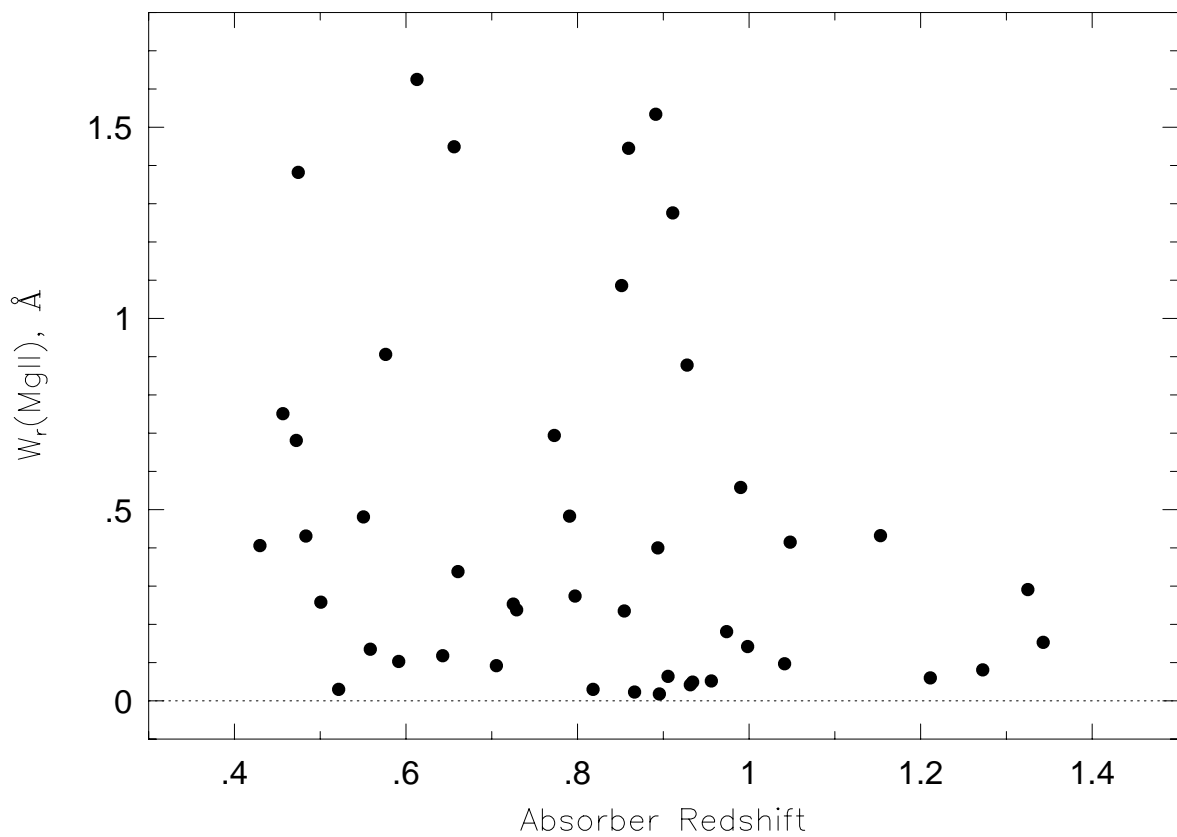


FIG. 1.— The rest-frame equivalent width of Mg II $\lambda 2796$ vs. absorption redshift for the sample.

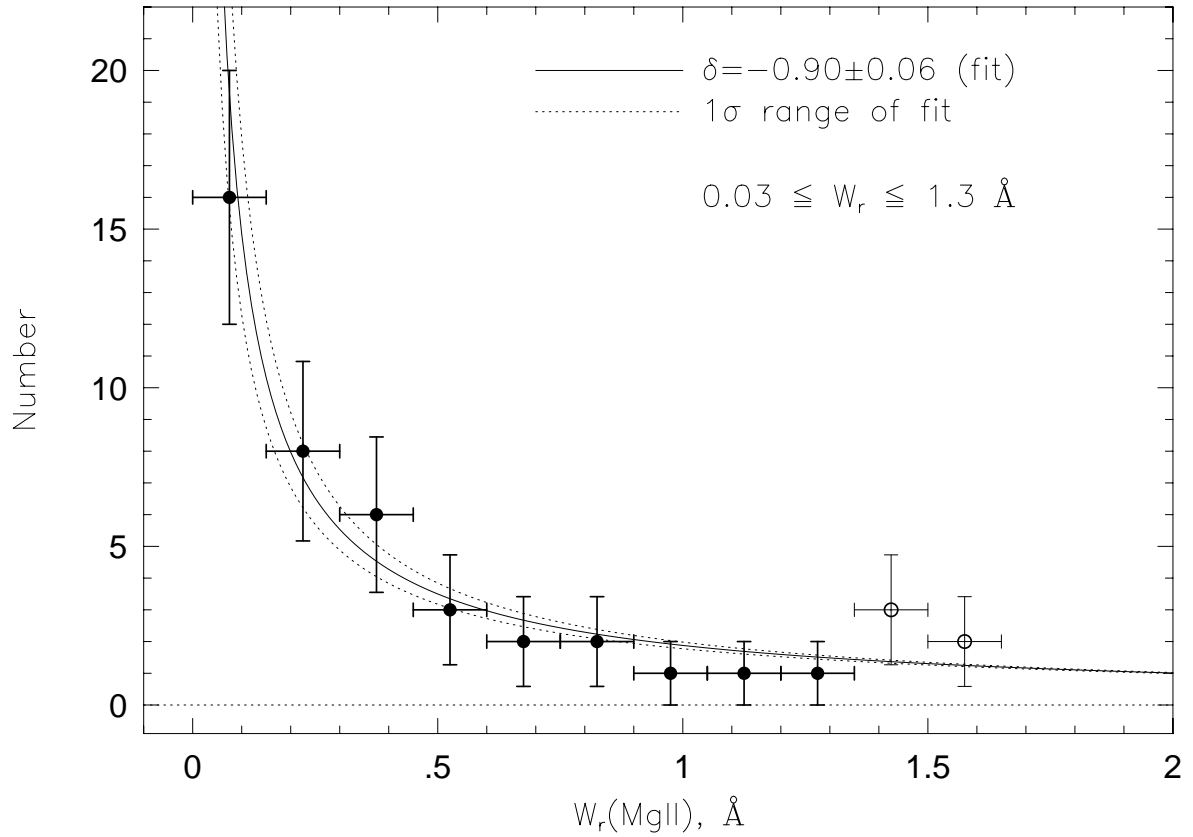


FIG. 2.— The rest-frame equivalent width distribution of Mg II $\lambda 2796$ for the sample. The data are binned at 0.15 \AA for presentation and given Poissonian uncertainties. The solid line is a maximum likelihood power-law fit (to the unbinned data) over the range $0.03 \leq W_r \leq 1.3 \text{ \AA}$. The dotted lines shows the 1σ range in the distribution function parameters. The unfilled data points were not included in the fit (see text).

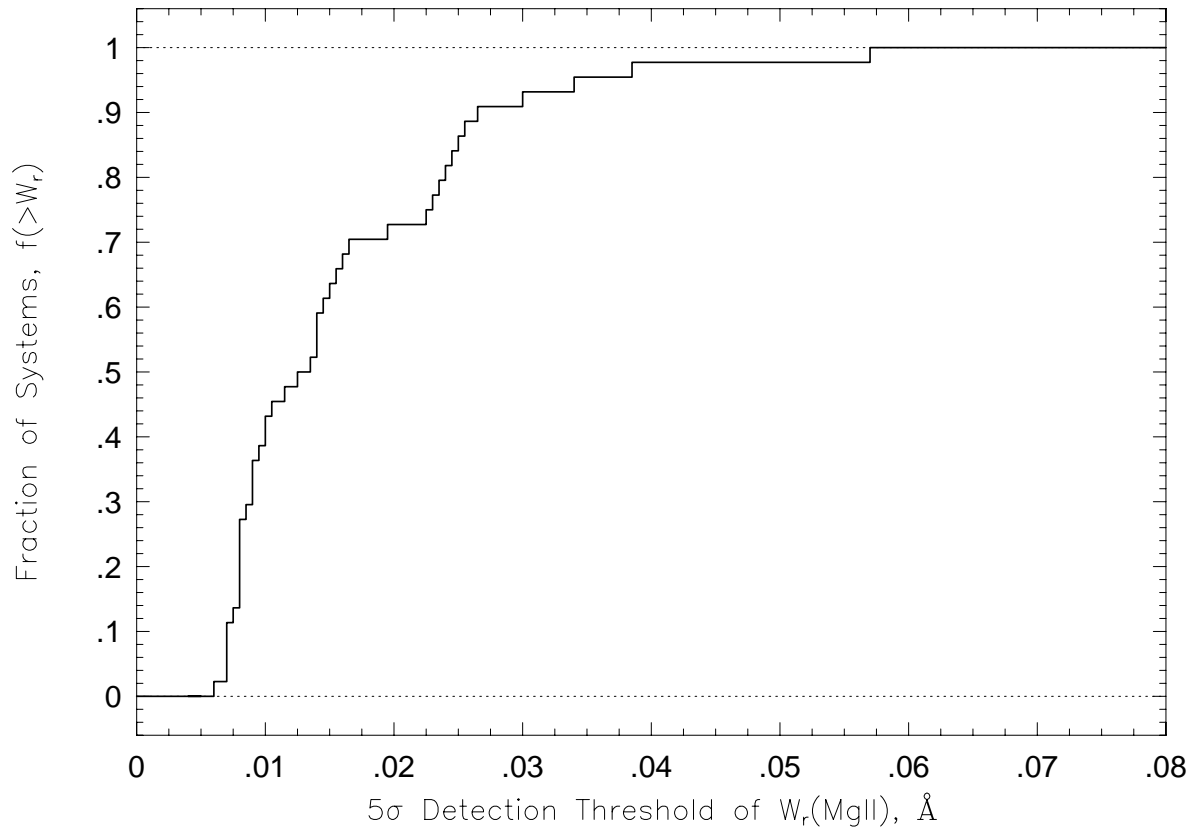


FIG. 3.— The cumulative distribution of the 5σ rest-frame equivalent width detection threshold of Mg II $\lambda 2796$ for the overall sample

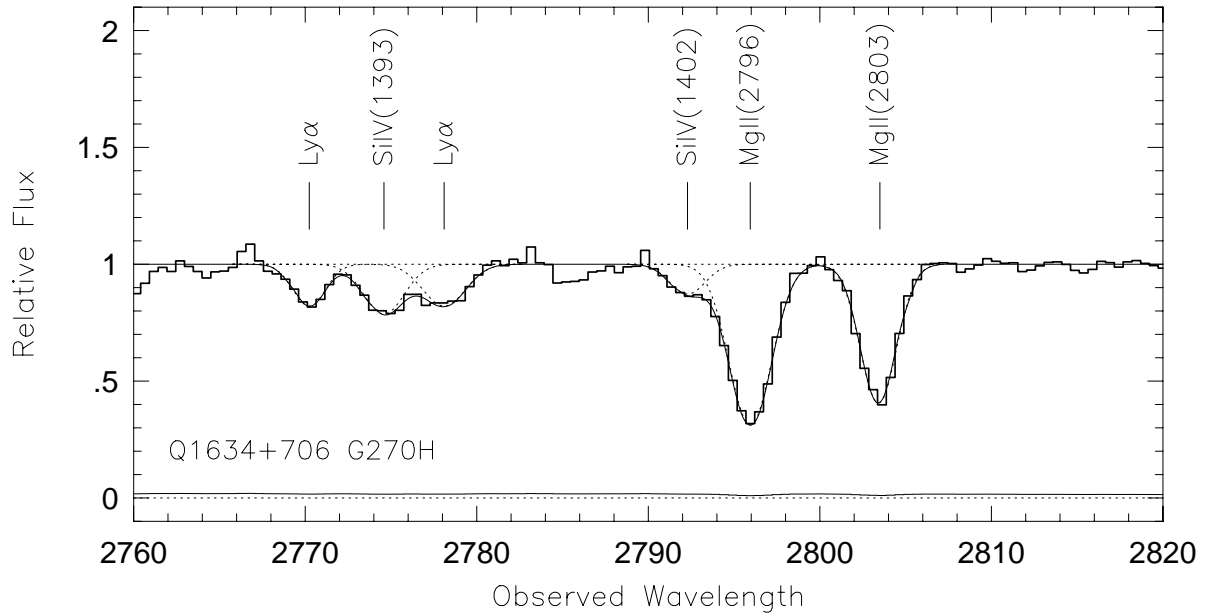


FIG. 4.— Example of Gaussian deblending to obtain equivalent widths from FOS spectra. Shown is the SiIV doublet at $z = 0.9902$ in the G270H spectrum of PG 1634 + 706; $\lambda 1393$ lies between two Ly α lines and $\lambda 1402$ resides in the wing of Galactic Mg II $\lambda 2796$.

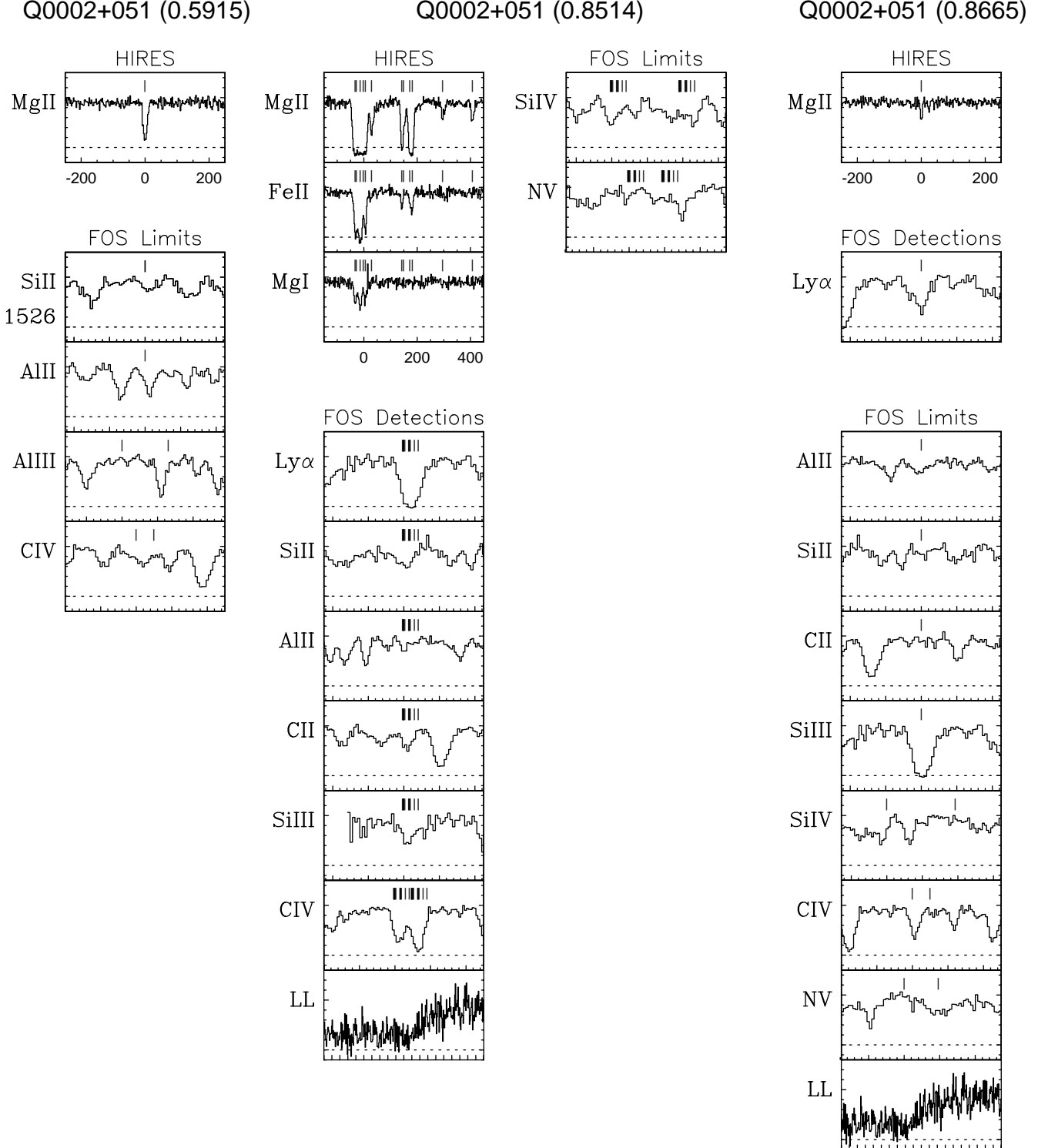
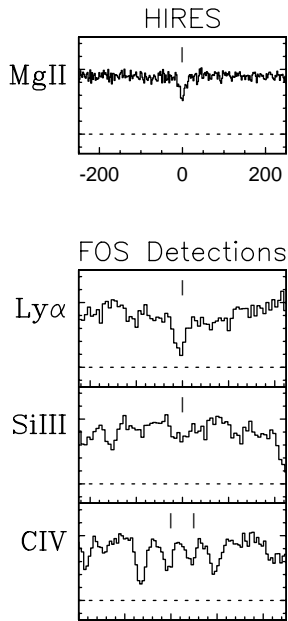
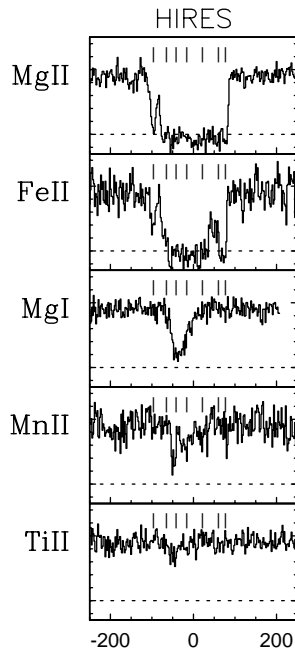


FIG. 5.— *a-ss*. For each system, the HIRES spectra of detected Fe II, Mg I, Ca II, and Ti II, and the FOS spectra of targeted transitions, separated by detections and non-detections. HIRES spectra ($\sim 6 \text{ km s}^{-1}$ resolution) span 500 km s^{-1} and are centered at the optical depth median integrated across the Mg II profile. FOS spectra ($\sim 230 \text{ km s}^{-1}$ resolution) are displayed in a larger velocity window of 4500 km s^{-1} , with small ticks on the horizontal axis separated by 200 km s^{-1} . The vertical ticks above the profile represent the different components of low ionization gas derived from Voigt profile decomposition of the HIRES profiles (see Paper II). The identical vertical ticks (derived from the HIRES data) are superimposed on the velocity scale of the FOS data panels, with a duplicate set of ticks for each member of the doublet transitions.

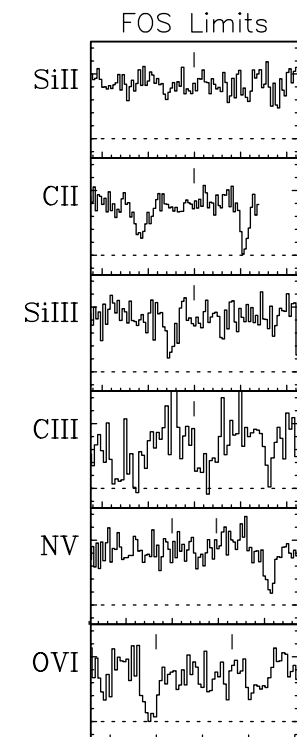
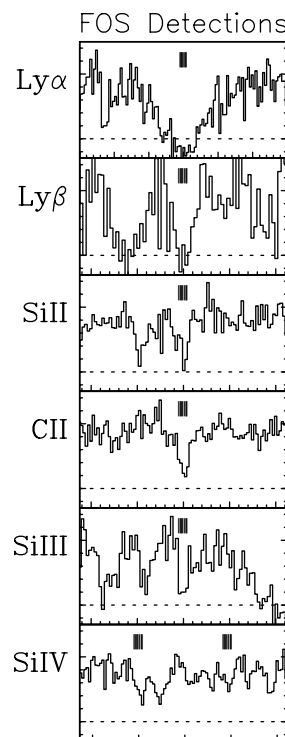
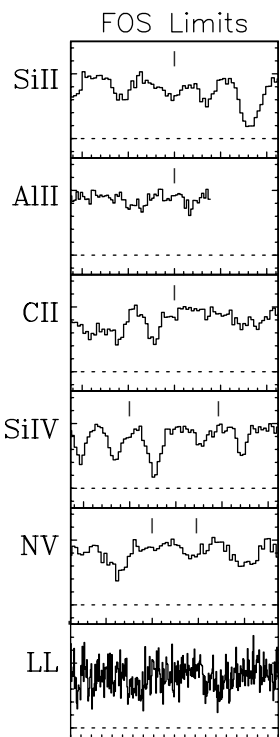
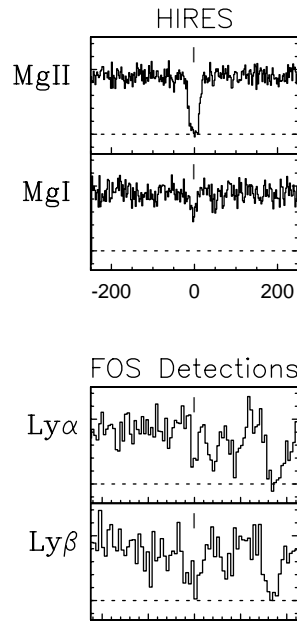
Q0002+051 (0.9560)

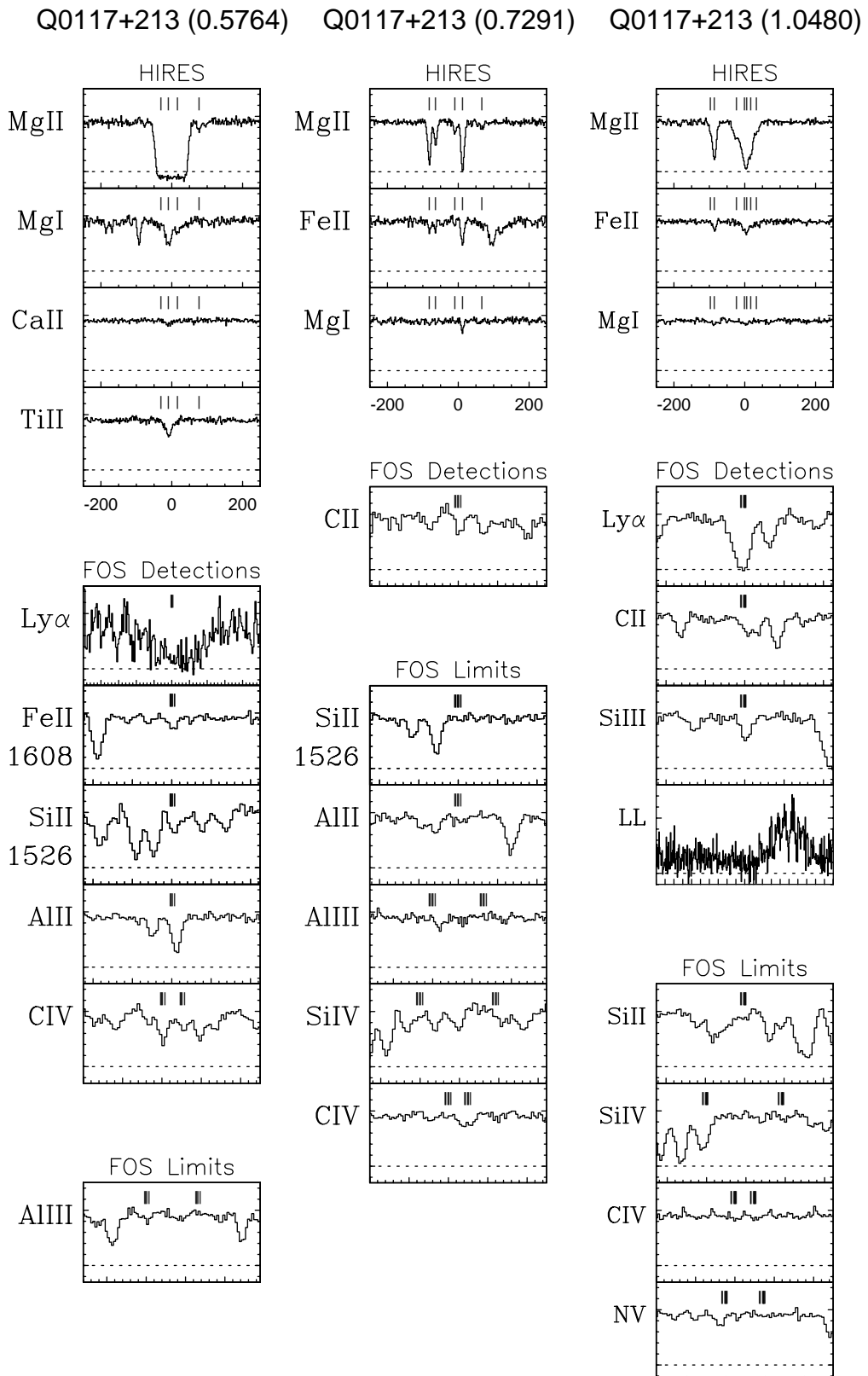


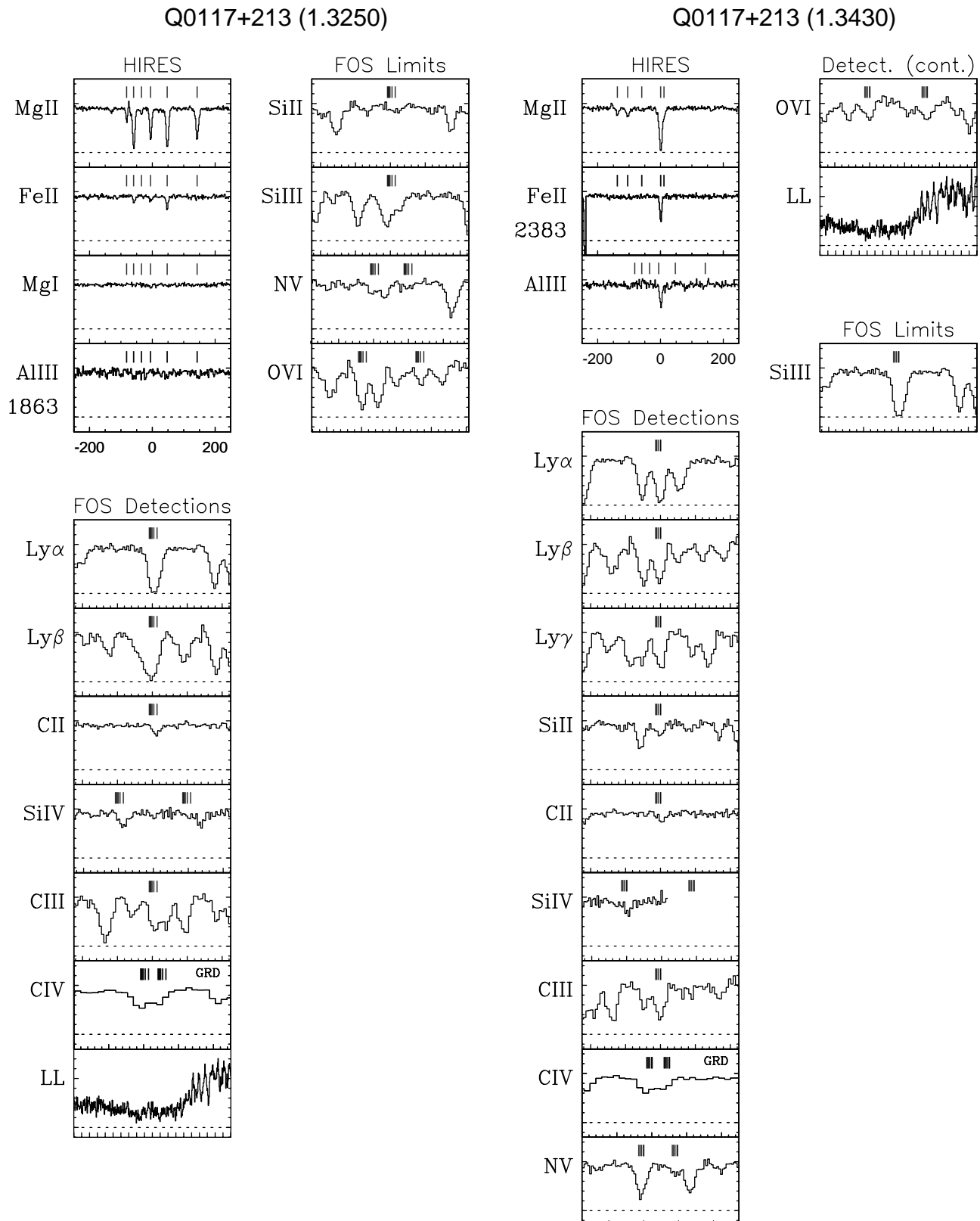
Q0058+019 (0.6127)

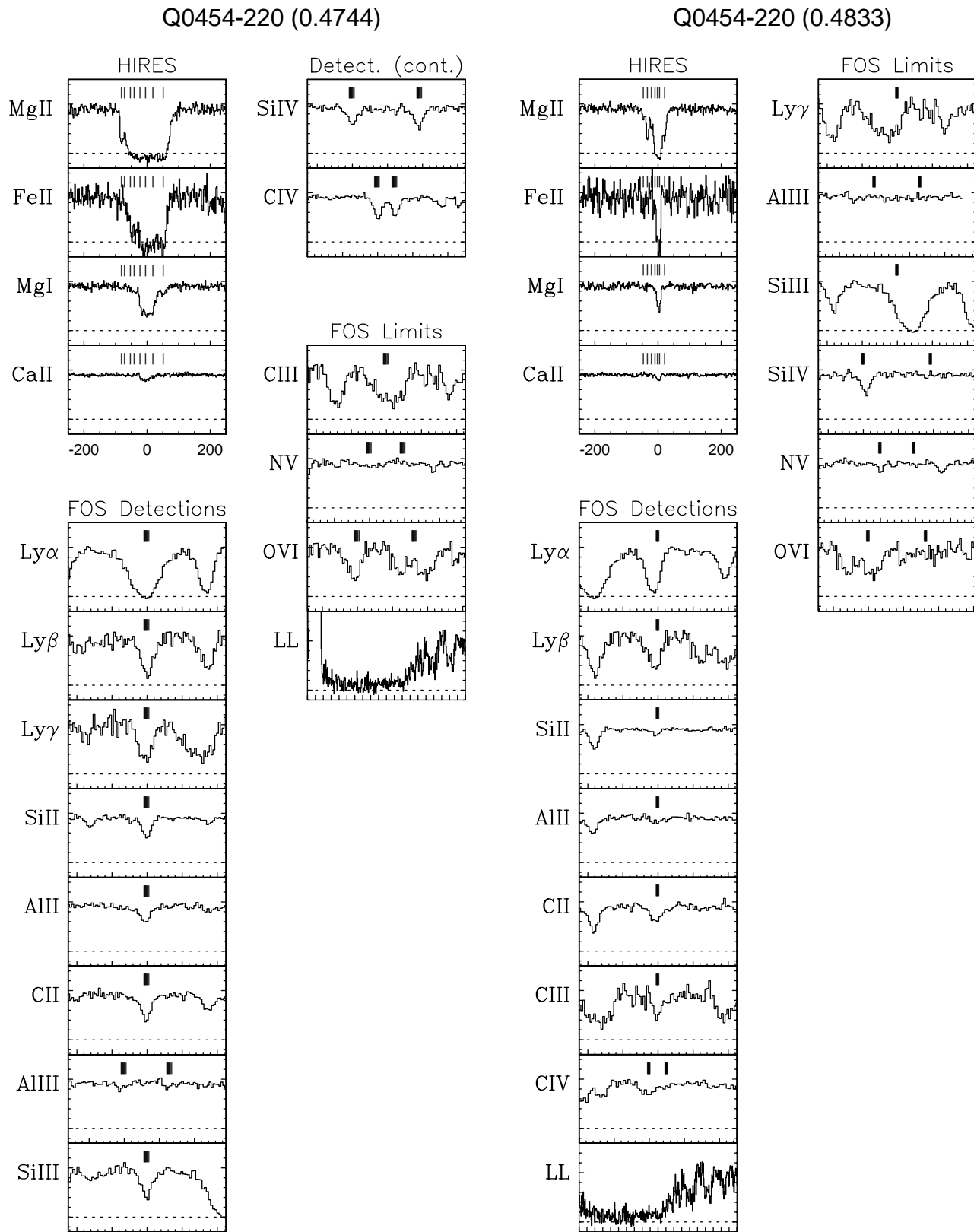


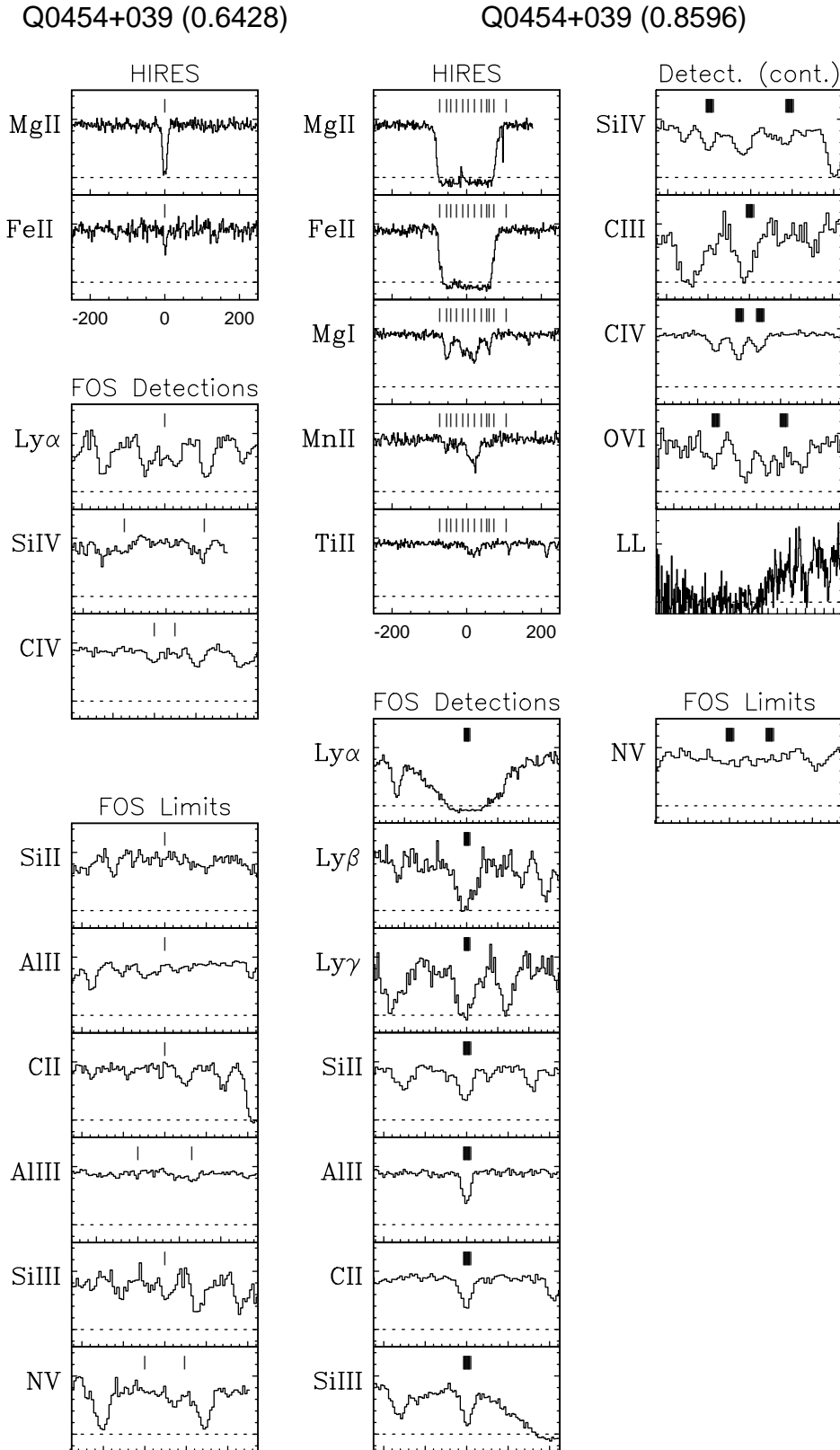
Q0058+019 (0.7252)

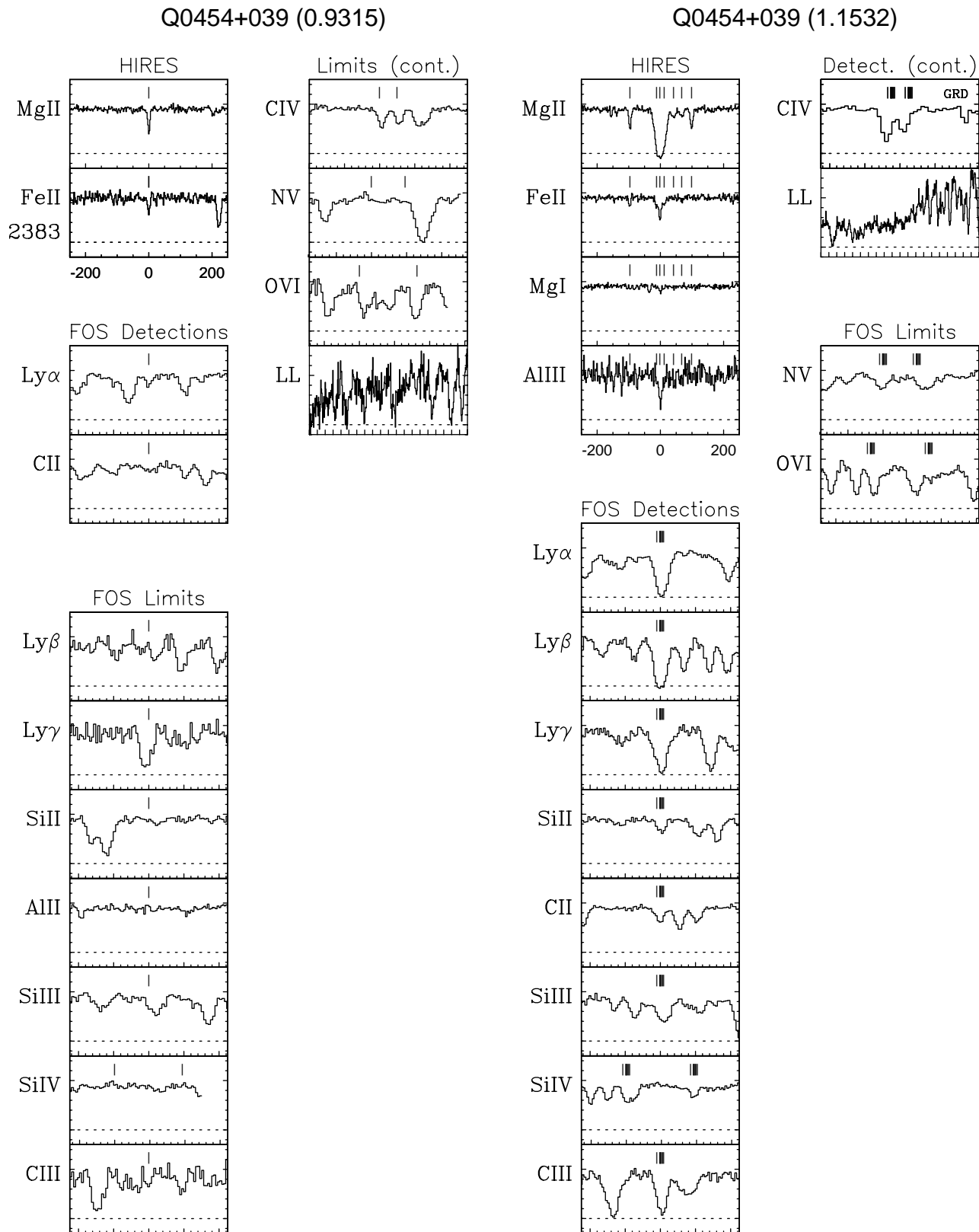


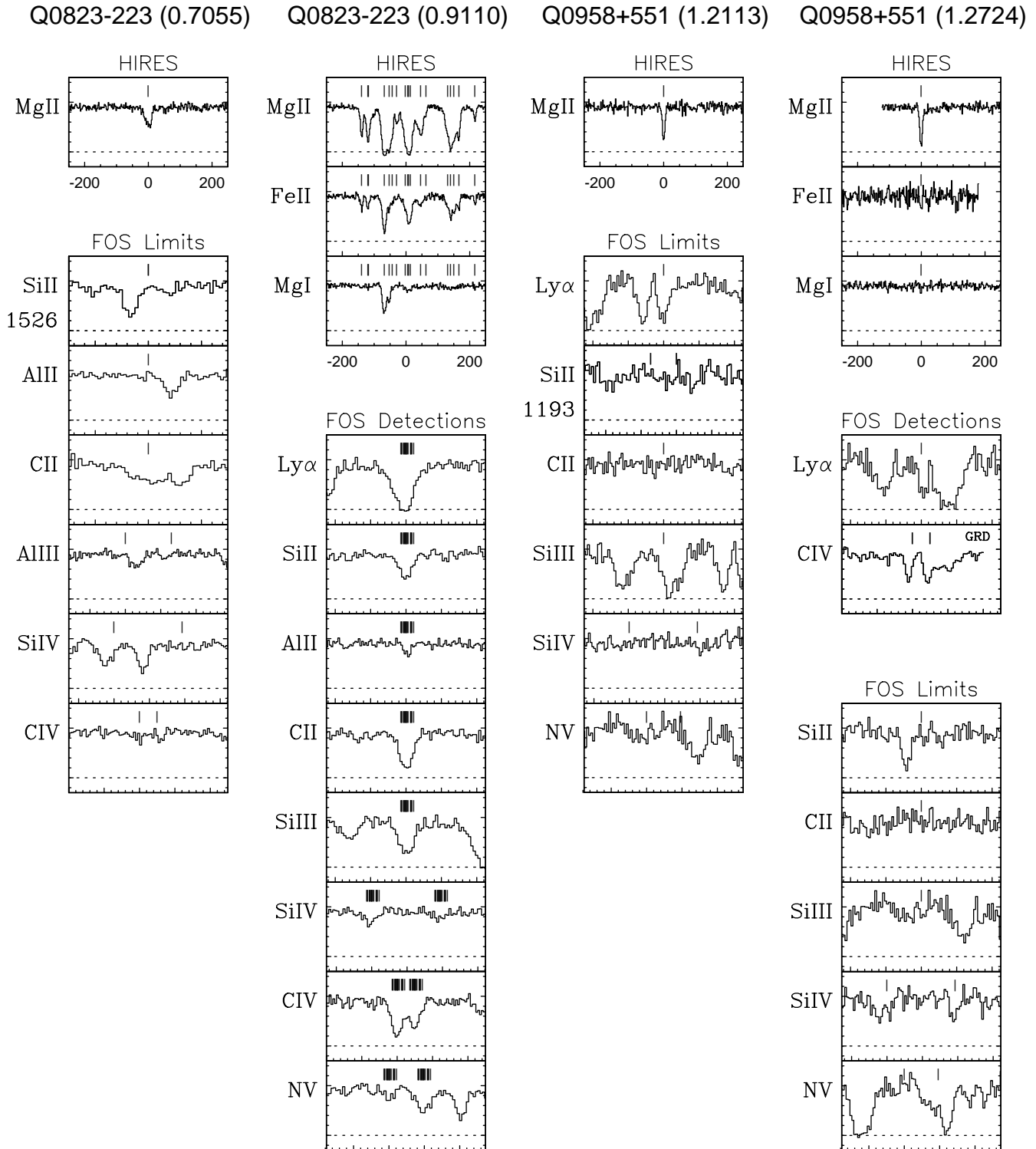


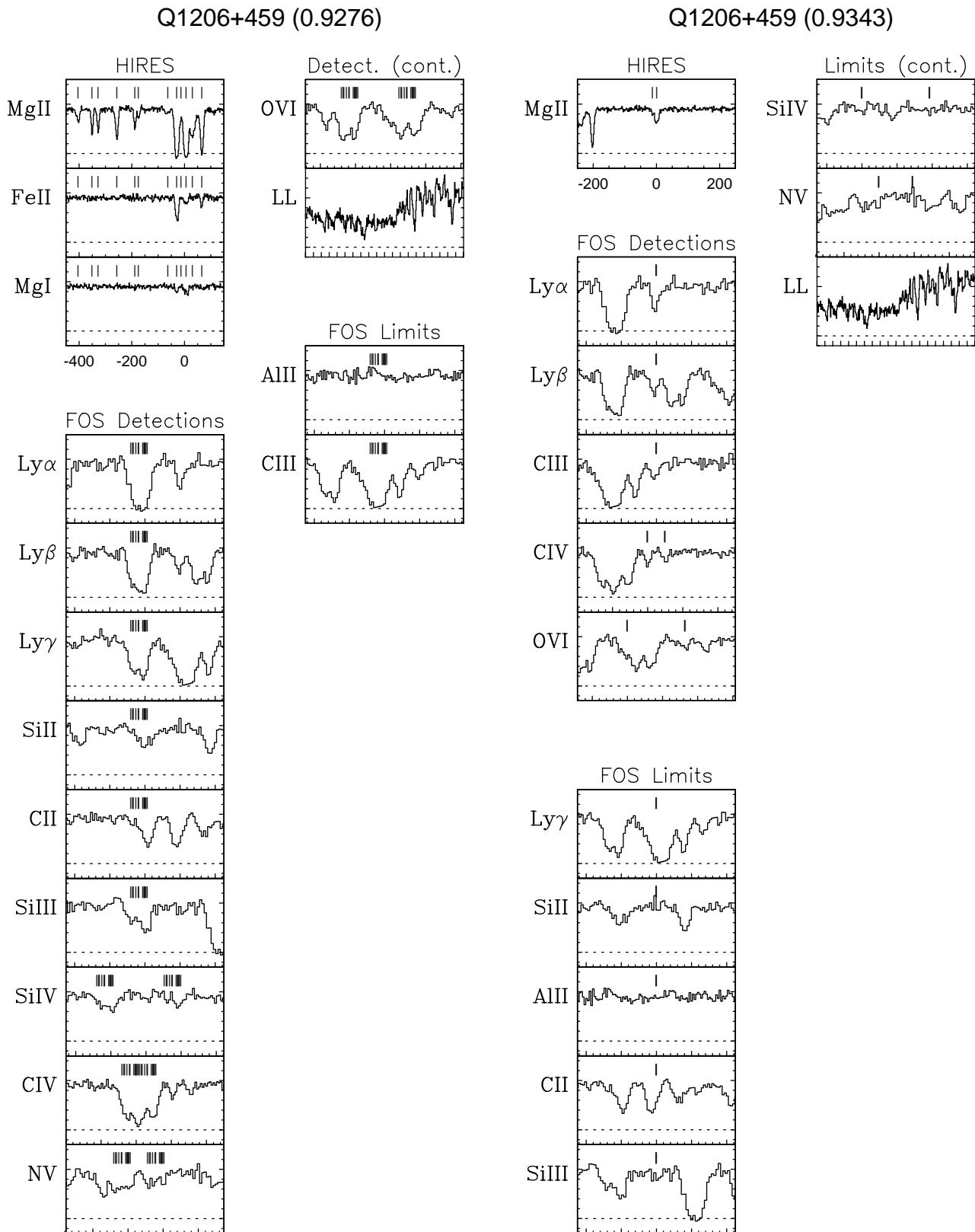


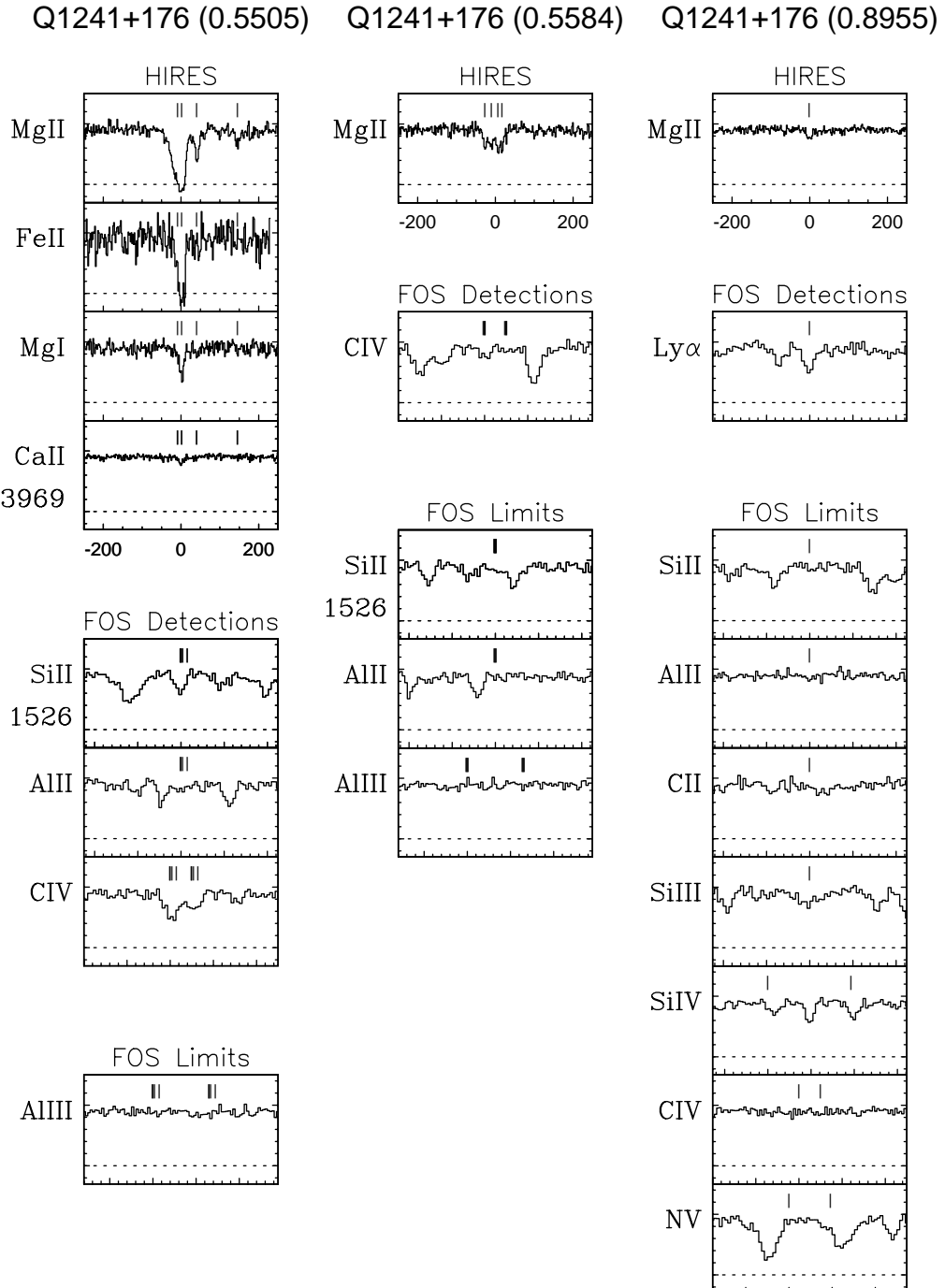


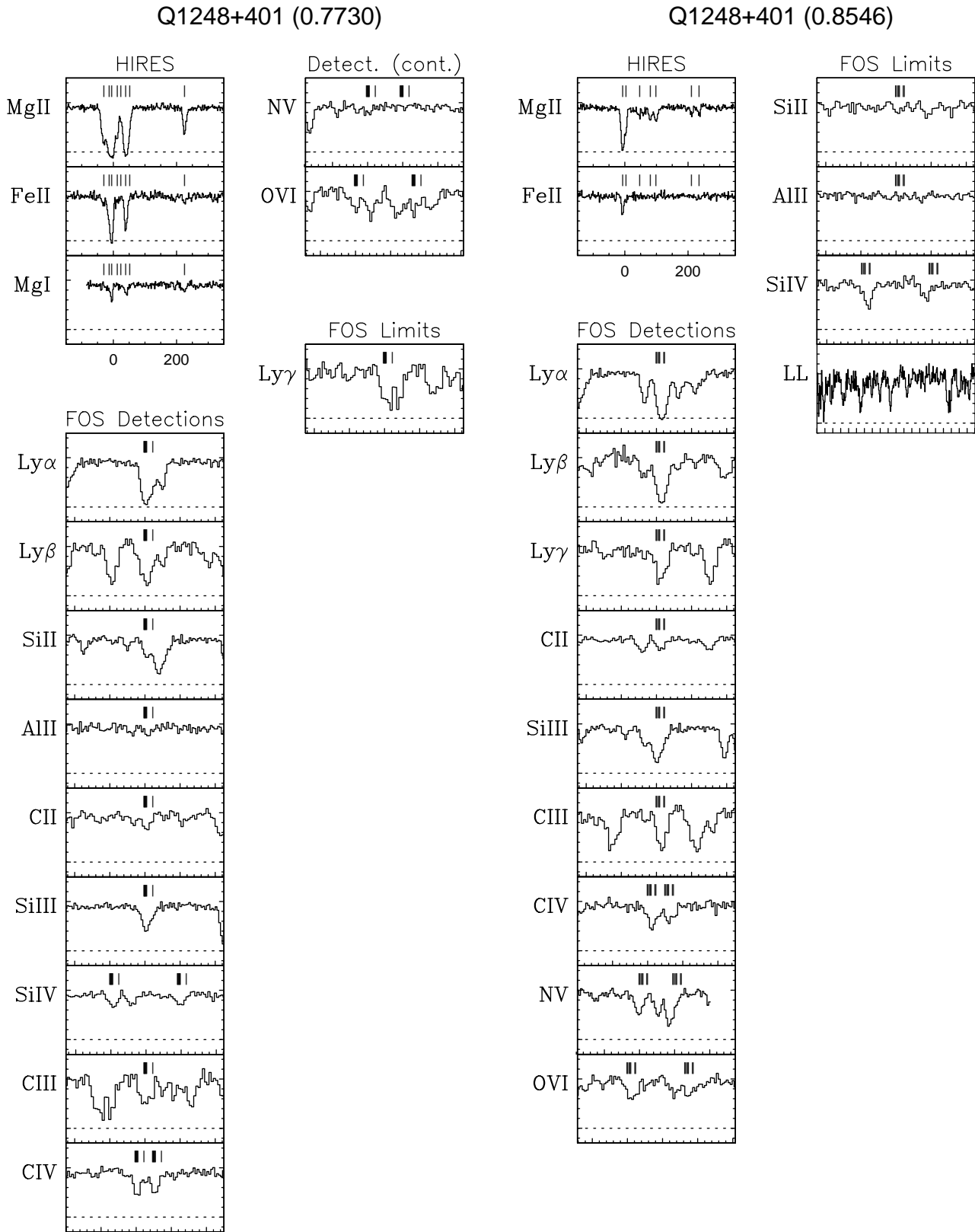


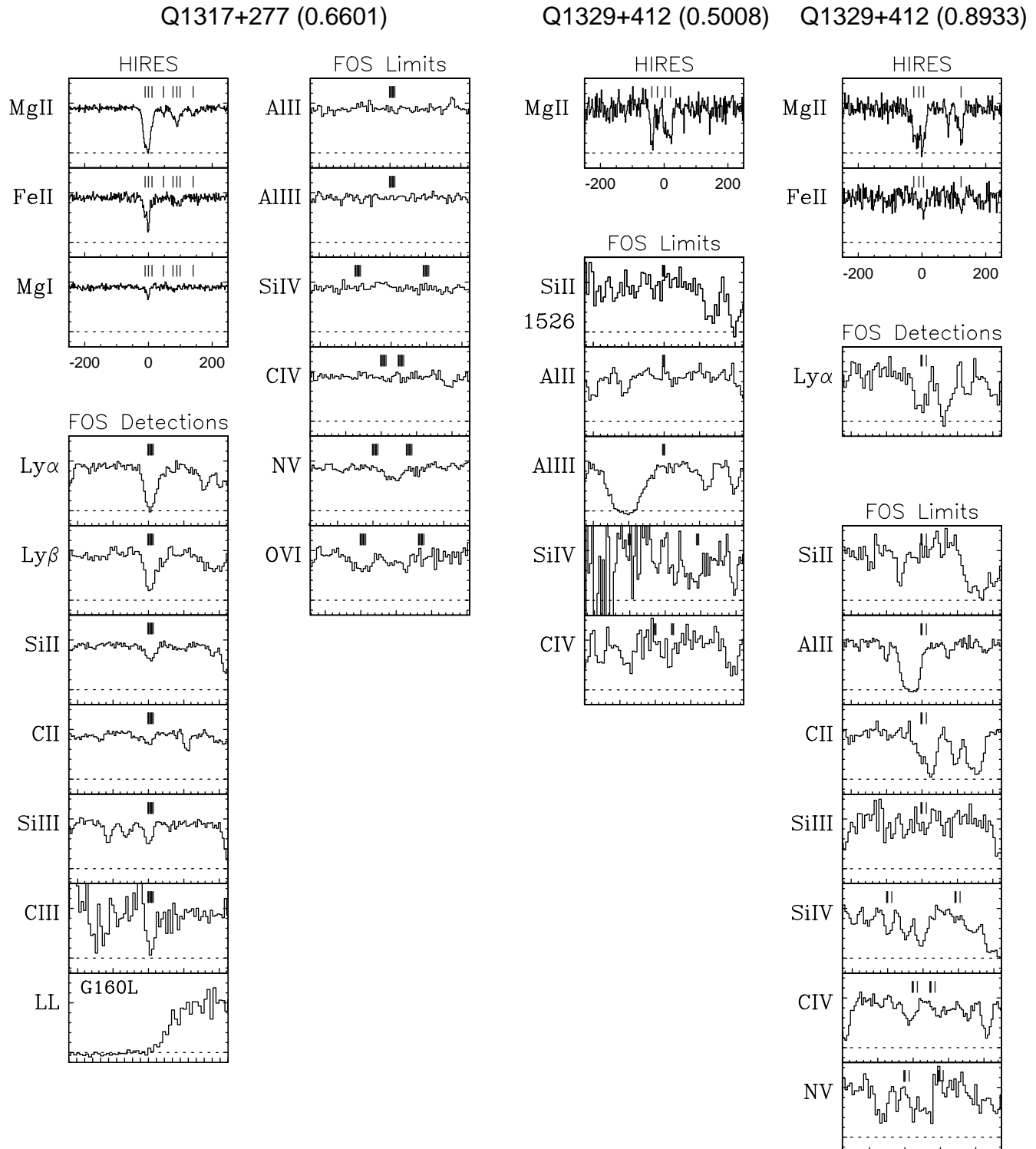


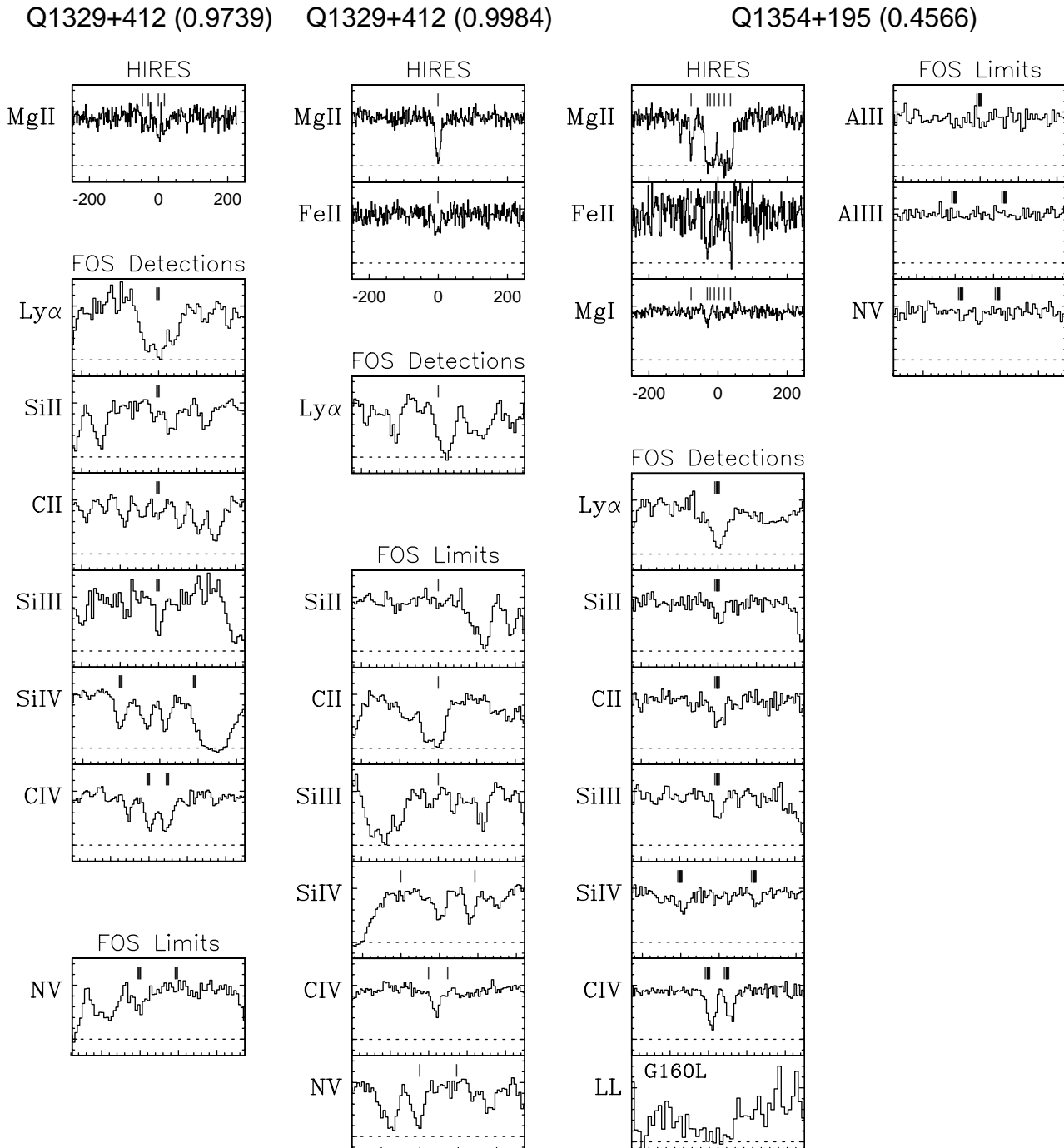


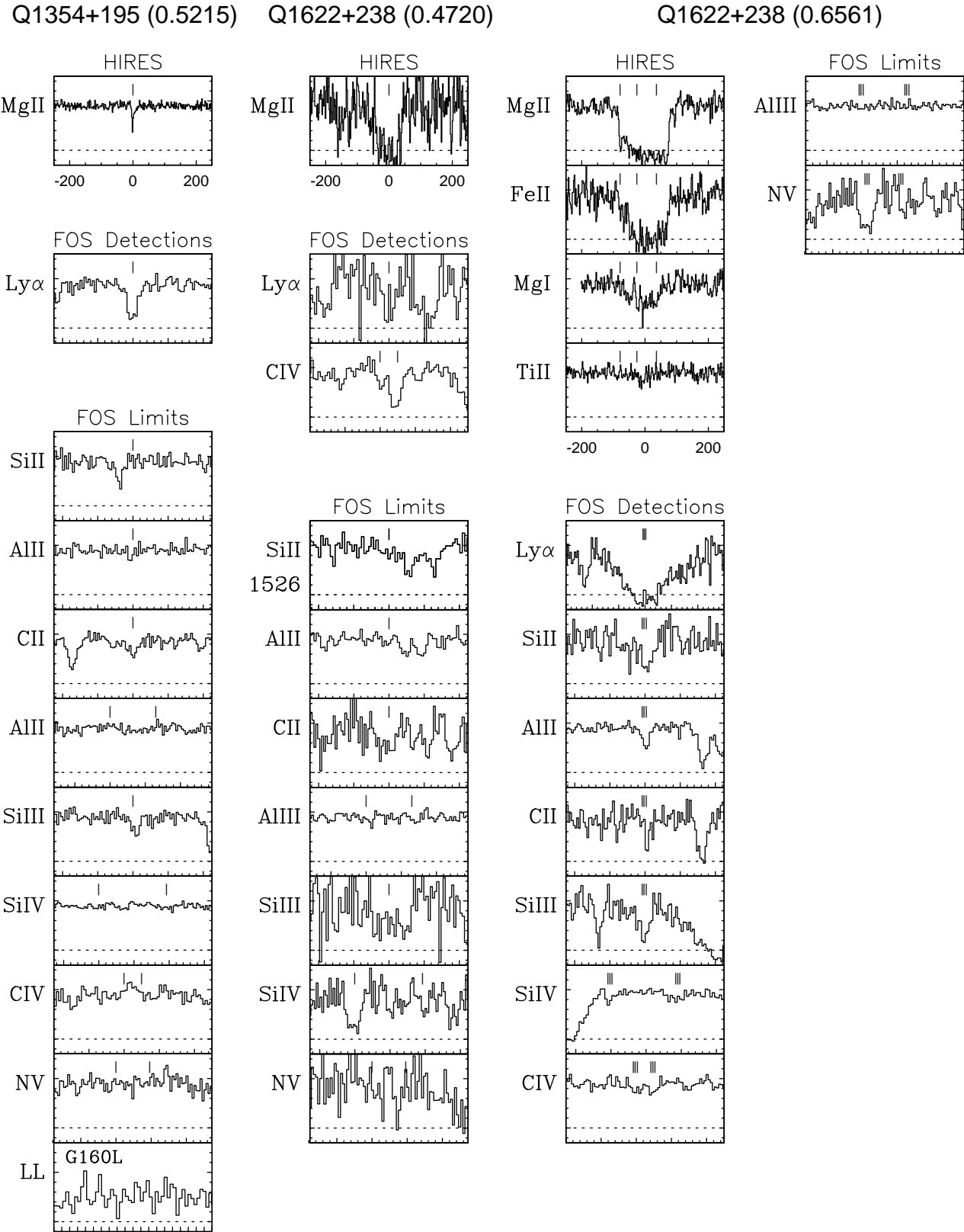


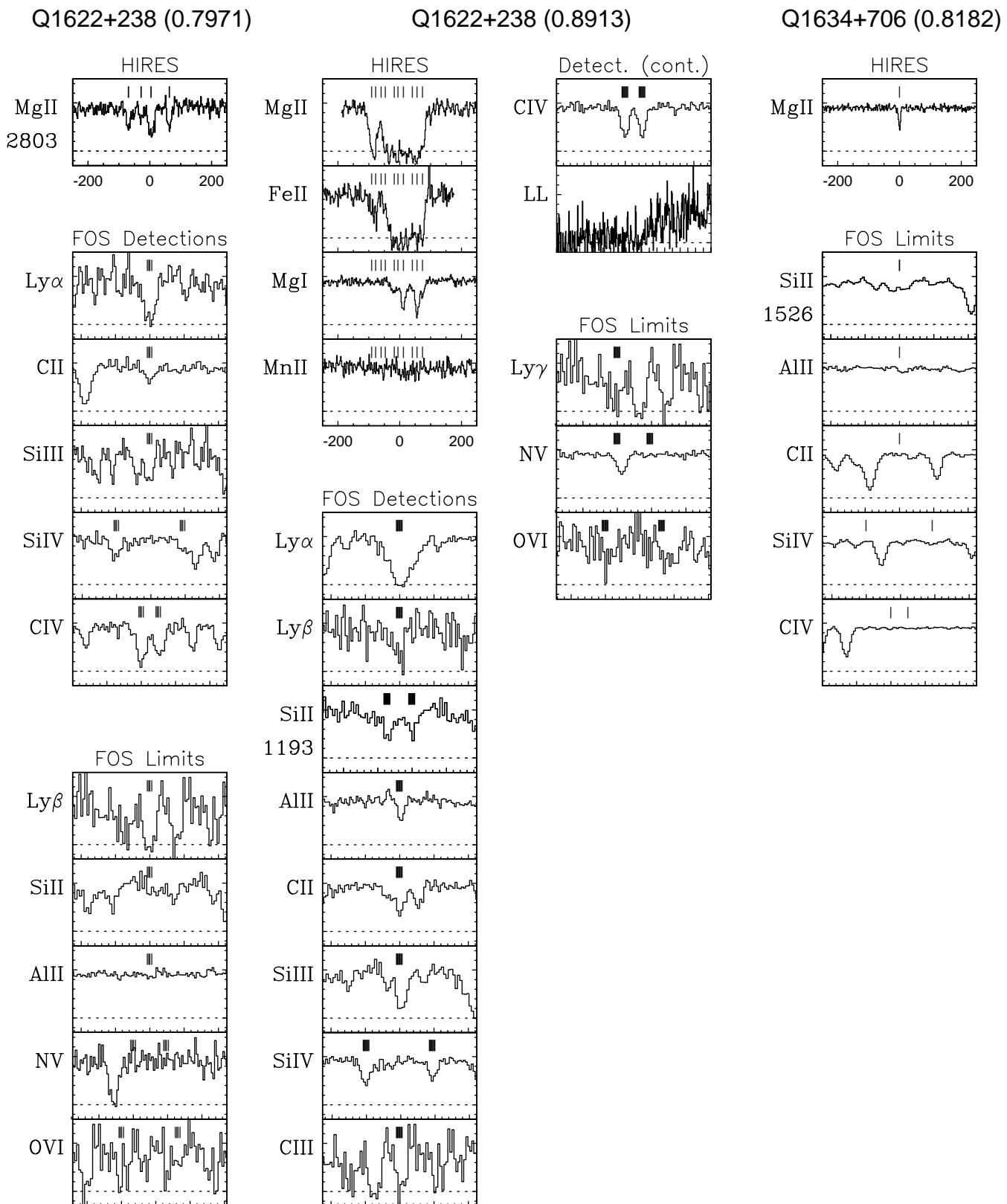


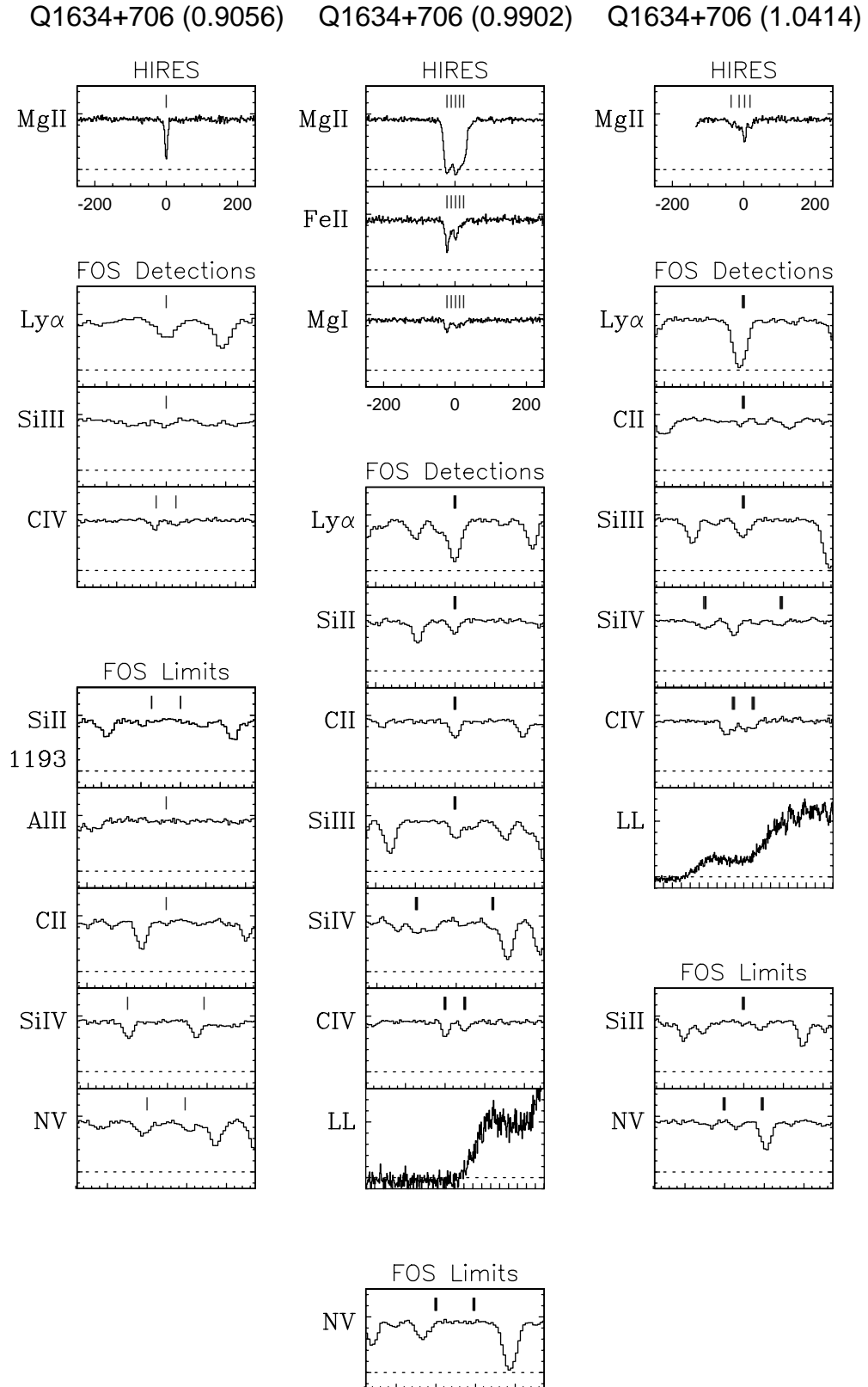


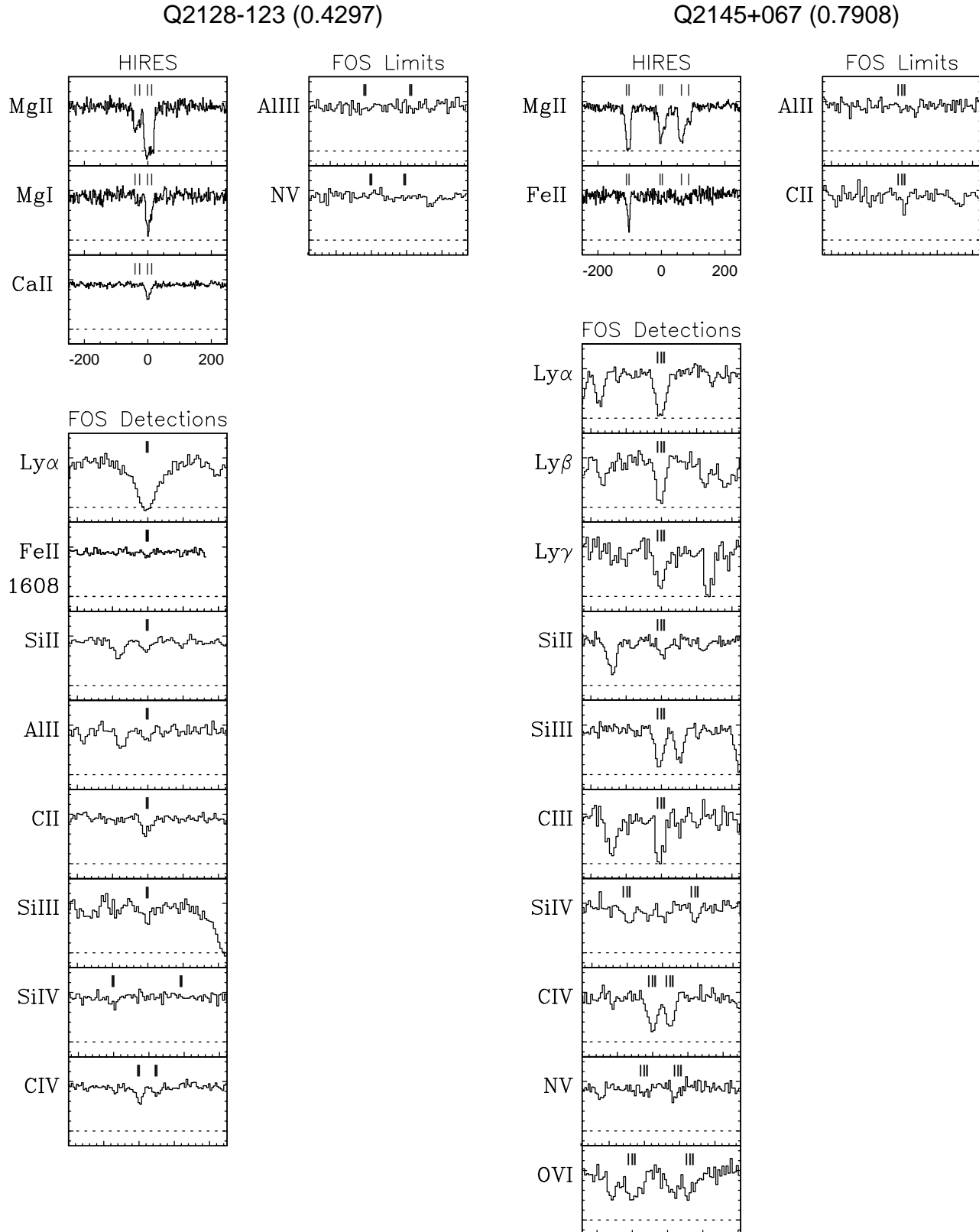












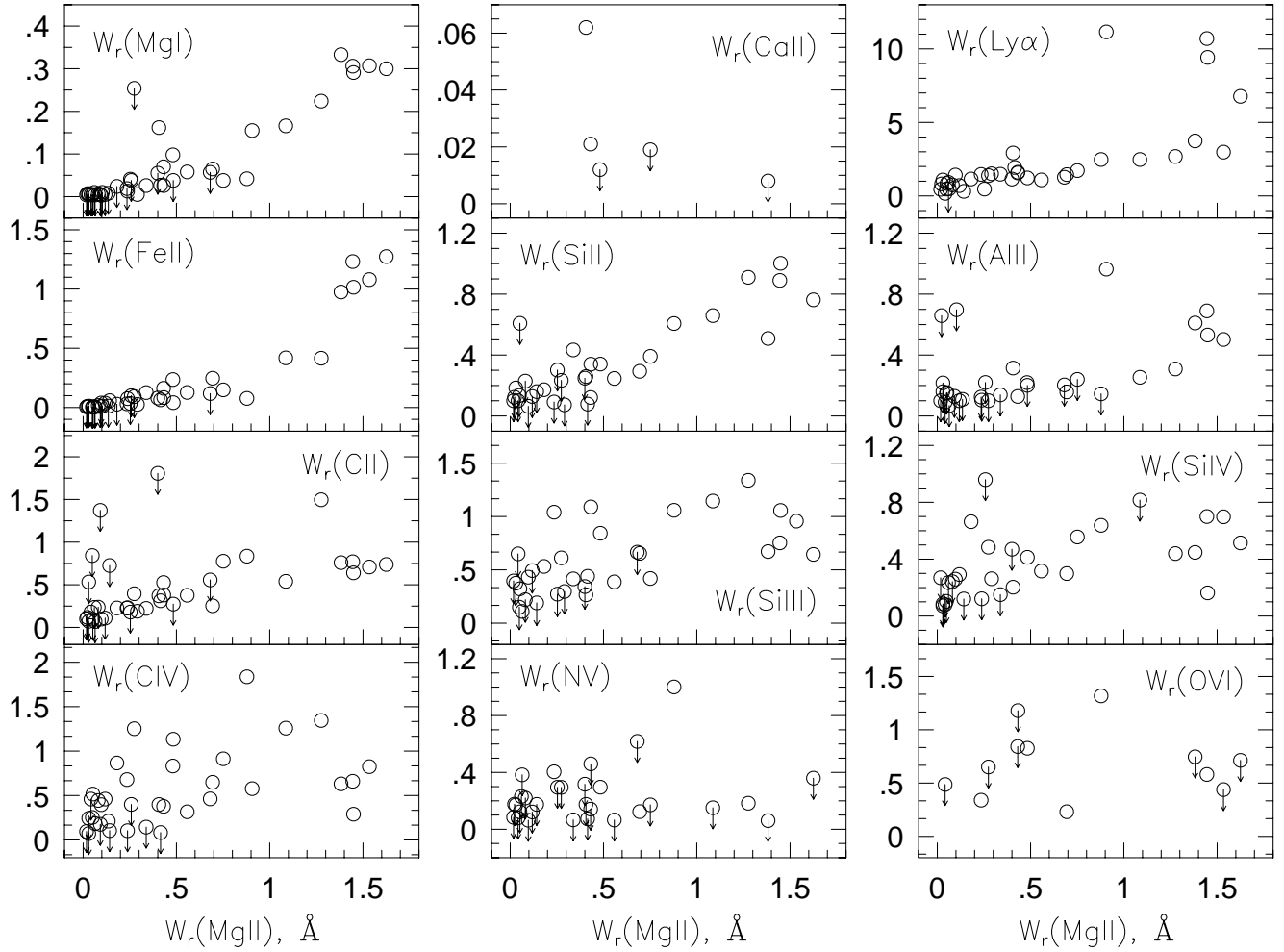


FIG. -10.— The rest-frame equivalent widths of the elemental species listed in Tables 3 and 4 vs. that of Mg II $\lambda 2796$. Also included is Ca II. The panels are in order of increasing ionization potential from the upper left to the lower right. Downward pointing arrows denote upper limits. Only “flag transitions” are plotted. If a measurement listed in Table 4 was based upon a transition other than the “flag transition”, it was not included.

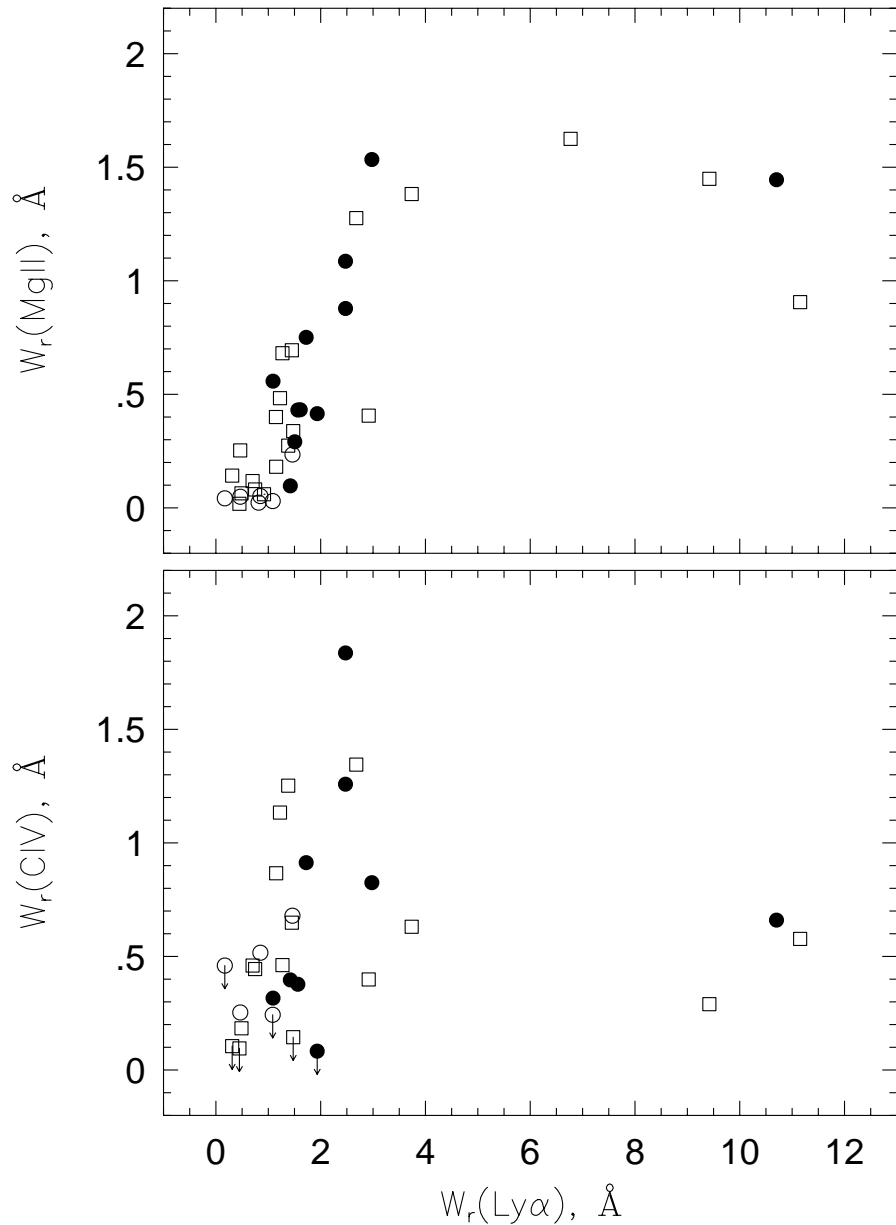


FIG. -9.— The rest-frame equivalent widths of Mg II and C IV vs. that of Ly α . The data point types are as follows: solid circles have measured Lyman limit breaks, open circles have no break measured, and open squares are systems for which the break was not covered. The median error of the data is roughly the size of the data points. Downward pointing arrows denote upper limits.

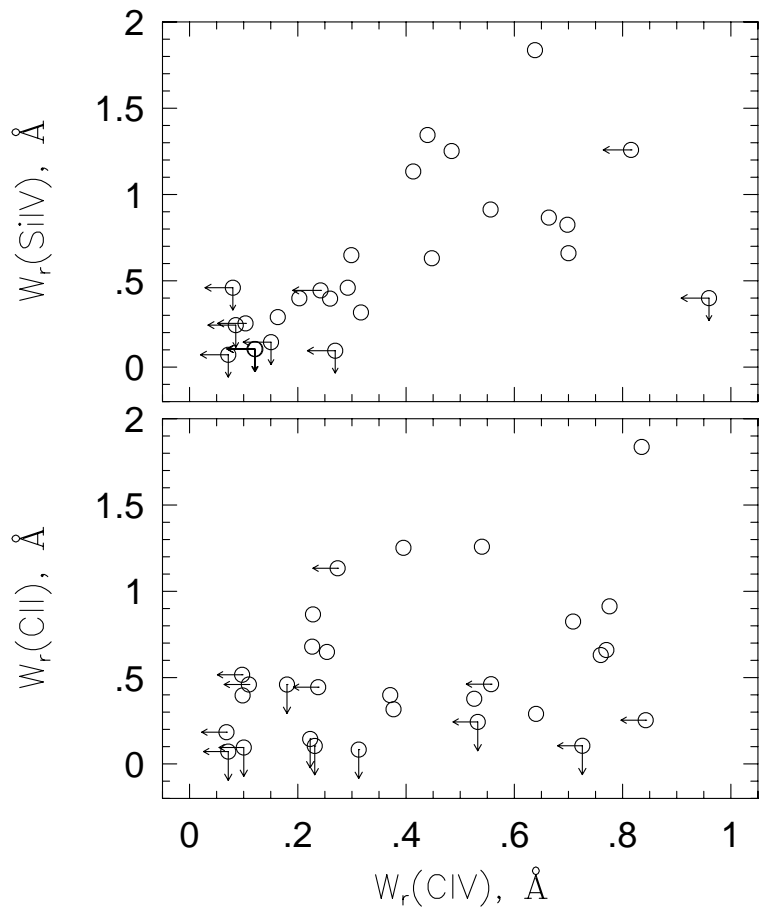


FIG. -8.— The rest-frame equivalent widths of SiIV and CII vs. that of CIV. The median error of the data is roughly the size of the data points. Downward pointing arrows denote upper limits on SiIV and CII, respectively, and leftward pointing arrows denote upper limits on CIV. Systems in which the “flag transition” was not measured are not included on this plot.

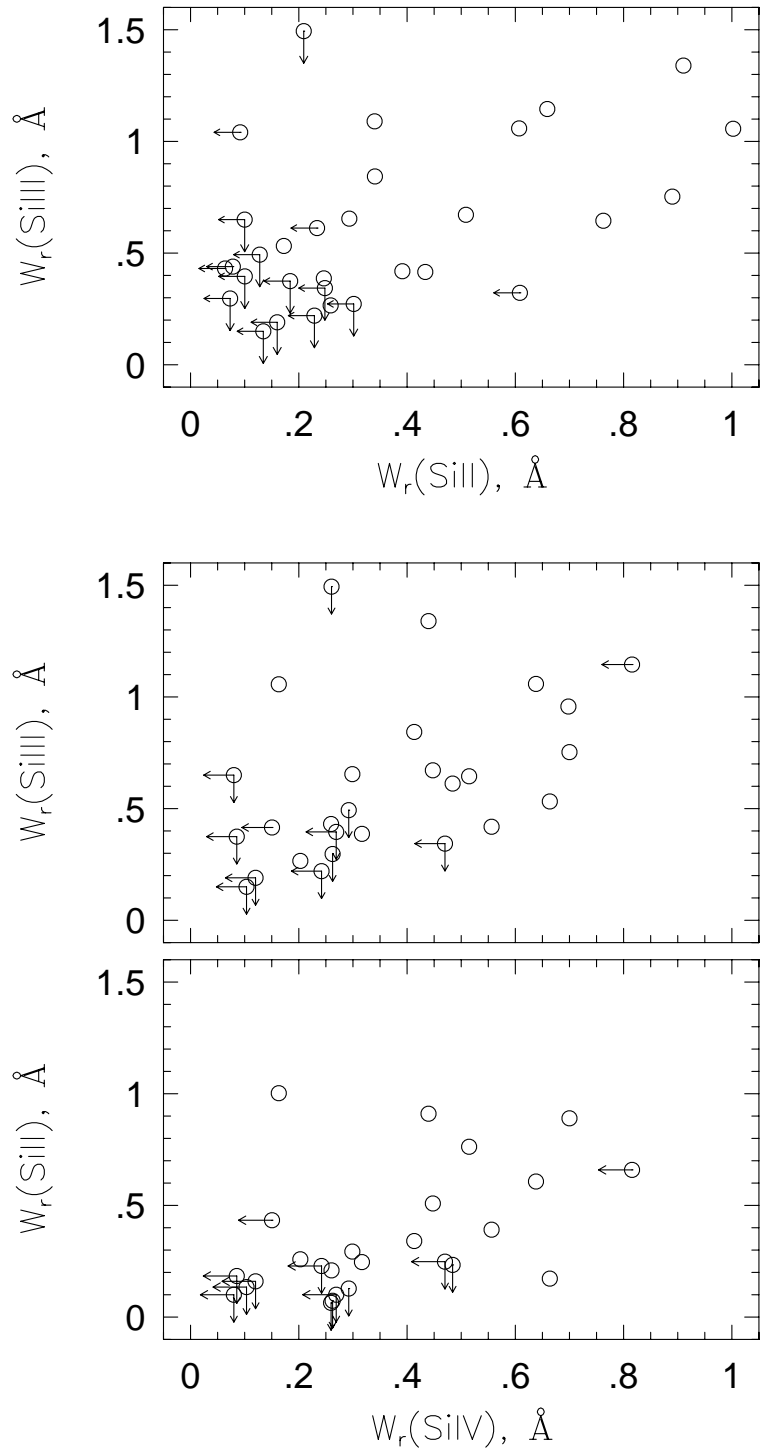


FIG. -7.— The rest-frame equivalent widths of Si III vs. Si II and of Si III and Si II vs. that of Si IV. The median error of the data is roughly the size of the data points. Downward pointing arrows denote upper limits on Si III and Si II, respectively, and leftward pointing arrows denote upper limits on Si II and Si IV. As with previous figures, only “flag transition” measurements are included.